



Polyamide-6 structuration induced by a chemical reaction with a polyether triamine in the molten state

M. Auclerc, A. Tauleigne, F. da Cruz Boisson, A. Vanhille Bergeron, N. Garois, R. Fulchiron, G. Sudre, P. Cassagnau, V. Bounor-Legaré

► To cite this version:

M. Auclerc, A. Tauleigne, F. da Cruz Boisson, A. Vanhille Bergeron, N. Garois, et al.. Polyamide-6 structuration induced by a chemical reaction with a polyether triamine in the molten state. *Polymer*, 2019, 172, pp.339-354. 10.1016/j.polymer.2019.03.033 . hal-02460276

HAL Id: hal-02460276

<https://hal.science/hal-02460276>

Submitted on 22 Oct 2021

HAL is a multi-disciplinary open access archive for the deposit and dissemination of scientific research documents, whether they are published or not. The documents may come from teaching and research institutions in France or abroad, or from public or private research centers.

L'archive ouverte pluridisciplinaire **HAL**, est destinée au dépôt et à la diffusion de documents scientifiques de niveau recherche, publiés ou non, émanant des établissements d'enseignement et de recherche français ou étrangers, des laboratoires publics ou privés.



Distributed under a Creative Commons Attribution - NonCommercial 4.0 International License

Polyamide-6 structuration induced by a chemical reaction with a polyether triamine in the molten state

M. Auclerc^a, A. Tauleigne^a, F. Da Cruz Boisson^b, A. Vanhille Bergeron^c, N. Garois^c, R. Fulchiron^a, G. Sudre^a, P. Cassagnau^a, V. Bounor-Legaré^{a,*}

^a Univ Lyon, Université Lyon1, Ingénierie des Matériaux Polymères, CNRS UMR 5223, 15 Bd Latarjet, 69622 Villeurbanne, France

^b Univ Lyon1, INSA de Lyon, Ingénierie des Matériaux Polymères, CNRS UMR 5223, 17 Av Jean Capelle, 69621 Villeurbanne, France

^c Hutchinson, Centre de Recherche, Rue Gustave Nourry - B.P. 31, 45120 - Chalette-sur-Loing, France

Corresponding author: veronique.bounor-legare@univ-lyon1.fr

HIGHLIGHTS

- A triamine agent can react with the polyamide-6 reactive functions by amidification and transamidification leading to branching points and chain scissions.
- The branching points created with a very small amount of triamine modified the crystalline nanostructure of the material as well as the lamellae thickness and content.
- These structural modifications were responsible for the higher T_g measured using the triamine reagent.

ABSTRACT

Polyamide-6 was modified by reactive extrusion using a triamine as a structuring agent. To scrutinize the reactive medium after the chemical modification and to characterize the new structures obtained, the coupling of several physico-chemical analyses was necessary and applied to either models molecules or polyamide chain. By correlation of liquid NMR, matrix assisted laser desorption ionisation/time of flight (MALDI-ToF), and size-exclusion chromatography (SEC) analyses, it was possible to observe both grafting and polyamide chain scissions that led to randomly branched and linear molecules. One of the most noticeable modifications regarding the properties was a decrease in the amorphous phase mobility with a very small amount of triamine (0.7wt%). A comprehensive study by X-ray scattering techniques (small and wide angle X-ray scattering, SAXS and WAXS, respectively) allowed us to highlight the noticeable size evolution of the crystalline and amorphous parts at the

lamellar scale. In conclusion, these multi-scale experiments demonstrate the possibility of modifying the amorphous phase mobility by controlling the nanostructure morphology of the material, particularly the crystalline lamellae thickness and the rigid amorphous fraction (RAF) content. Thus, an increase in the RAF content of around 6% induced more restricted mobility in the amorphous phase as the glass transition temperature (T_g) shifted to higher temperature ($\approx + 7\text{ }^\circ\text{C}$).

1.1. Introduction

Polyamide-6 was one of the first synthetic polymers industrialized more than 60 years ago and it remains largely produced particularly for the automotive industry which attempts to replace metal in a large number of applications. This replacement is possible thanks to its attractive properties such as; good mechanical strength, high temperature resistance, and excellent resistance to chemicals. But the main limitation is moisture absorption and the resulting degradation of its mechanical properties. It is also well established that polyamide-6 exhibits high notch sensitivity at low temperature. In order to use polyamide-6 in drastic conditions like under-hood and in load bearing applications, physical and chemical modifications are usually required. Among them, many studies discuss the incorporation of fillers [1-3] and polymer blending [4-7] or chemical modifications (chain extensions [8-12], incorporation of branched structures into the polymer [13]...). The latter solution was chosen in this work. For the chains extensions, three main functions have been widely used in the literature such as bis-oxazoline, epoxide and bis-caprolactam leading mainly to the enhancement or conservation at least of the mechanical properties. Furthermore, as a consequence of the molar mass increase, the viscosity is always enhanced dramatically.

As an alternative to this issue, new chemical structures were developed including branched structures by direct synthesis of branched/hyperbranched polyamide or introduction of a small amount of branched/hyperbranched molecules as additive into the polyamide matrix. These structures in very small amounts led to unusual properties as lower viscosity (compared to the one of linear polymer with equivalent molar mass) and equivalent or improved mechanical properties. As an example, Huber et al. [13] studied the modification of polyamide-6 with a small amount of hyperbranched poly(etheramide). Addition of 0.1 to 10 wt% of hyperbranched poly(ether amide) in a polyamide-6 (B01 to B10) matrix was carried out at $250\text{ }^\circ\text{C}$ with a twin-screw mini-compounder. As expected and proved elsewhere, the addition of small amount of hyperbranched into the polyamide, reduced the complex viscosity compared to the pure PA-6 even at very low concentrations (from 800 to 600 Pa.s adding 0.1 wt% of hyperbranched poly(etheramide)). Dynamic mechanical analysis results displayed an increase of the glass transition from $53\text{ }^\circ\text{C}$ to $59\text{ }^\circ\text{C}$ with only 1 wt% of the hyperbranched polymer. Finally, for the same concentration, the shear storage modulus was significantly higher between 50 and $150\text{ }^\circ\text{C}$.

If the viscosity loss is often explained by the reduction of entanglements between polymer chains, the contradictory better mechanical properties values are hardly ever discussed. The fundamental comprehensive structure-properties relationship often remains at the hypothetical stage. In semi-crystalline polymers, in addition to combining outstanding properties of various materials, modification of the crystalline structure is often the key to explain the macroscopic properties evolution. Indeed, for many years, research work has investigated the link between final macroscopic properties and structural parameters including the degree of crystallinity [14-17], the lamellar orientation and thicknesses [18, 19], and the spherulite size [20].

Most of the studies have described a direct relationship between the mechanical properties and the crystalline morphology. As an example, Menyhárd et al. [18] studied the crystalline structure and mechanical properties of synthetic isotactic polypropylene with diverse molecular structures (molar mass, polydispersity and chain regularity). By correlating differential scanning calorimetry (DSC), WAXS and tensile test analyses, the results demonstrated that both higher crystallinity and thicker lamellae thickness induce better stiffness with a non-linear correlation. As an example, with thicker crystalline lamellae (from 15 to 20 nm) and higher crystallinity (from 46.7 to 67.9%), the Young's modulus and yield strength increased by 1.1 GPa and 15 MPa, respectively. The authors determined that the crystalline lamellar thickness and the crystallinity are independent parameters [15]. In addition to these observations, several research teams developed models to predict the mechanical properties when the structural parameters are known [21-22]. Among the most recent and complete studies, Fatahi et al. [23] established a comprehensive model for polyethylene that correlates the experimental tensile modulus with micro- and nano-structural parameters like crystallinity, crystal size, lamellar thickness and length, orientation factors, and long spacing period obtained from different techniques. The mechanical properties in both the MD (machine) and TD (transverse) directions were measured on different polyethylene blown films and compared to the calculated properties. A reasonable agreement was found between values obtained with the model and the experimental data. Finally, Stern et al. [24] reported a very detailed study about the influence of the crystalline morphology and the weight-average molar mass on the Young's modulus and the tensile stress. Modifications regarding the crystallinity were studied for polypropylenes with different molar masses (100-1600 kg.mol⁻¹) and processing conditions (temperature and pressure). They proved that both thicker crystalline lamellae and/or smaller amorphous lamellae could improve the Young's modulus. As an example, when a sample was annealed for 1 h at 140 °C, a thickening of the crystalline lamellae by 3 nm (from 22.5 to 24.7 nm) was observed, and a lower degree of crystallinity (by 4%) was obtained by increasing the molar mass of the polypropylene from 320 to 1120 kg.mol⁻¹. The Young's modulus (at 0.05% strain) was enhanced from 1820 to 2160 MPa as the crystalline layer thickness governs the tensile properties. In this case, the well-known linear relationship between crystallinity and mechanical properties was not verified as the molar mass was modified significantly.

Compared to the mechanical properties, only a few studies have explained the amorphous phase mobility evolution in terms of crystalline parameters. The T_g is often related to the mobile amorphous fraction (MAF), the rigid amorphous fraction (RAF) and the amorphous phase thickness, considering the material as a three-phase model. Regarding this problem, the effects of the amorphous layer thickness on the T_g were investigated on a semi-crystalline PET by Dobberty et al. [25]. The fraction of amorphous phase (rigid or mobile) and crystalline phase was estimated by DSC, while the lamellae thickness was studied by SAXS with a one-dimensional layer stack model after various thermal treatments. They introduced the term of “cooperative length” (CRR), which was defined as the minimum space required to enable a segment of chain to undergo a transition to a new configuration after a sufficient sollicitation. If the thickness of the amorphous lamellae is smaller than this length (from 1 to 3 nm), the relaxation is broader and the T_g shifts to higher temperatures. By dielectric measurements, it was proved that the dynamic glass transition temperature increased when the mobile amorphous layers became thinner. Dobberty and his team, Picciochi et al. [26], and Hong et al. [27] confirmed a direct link between the thickness of the mobile amorphous lamellae and the glass transition temperature for semi-crystalline polymers. To go a step further, they used a model suggesting that the thickness of the rigid amorphous layer also influences the T_g as it possesses some degrees of freedom. If this later phase does not exist, the mobile amorphous phase is directly in contact with the rigid crystalline layer preventing some segmental motion (increasing T_g). In contradiction with this latter study, quite a few teams considered the rigid amorphous fraction as a phase which brings rigidity and molecular mobility restrictions in the amorphous phase. The confinement of the mobile amorphous phase by the RAF has been reported in several papers [28, 29]. For example, the linear increase of the glass transition temperature of polyamide-6 with the RAF content was recently described by Paroli et al. [30]. The relation was not linear, but between a RAF content of 20% and 40%, the T_g increased from 70 to 80 °C.

The influence of the crystalline layers' thickness on the T_g is poorly documented. As an example, Charlon et al. [29] explained a higher glass transition temperature obtained on a semi-crystalline biodegradable polyester [(poly(butylene succinate))] with the crystalline lamellae thickness and/or the rigid amorphous fraction. Indeed, larger crystalline lamellae and higher rigid amorphous phase content might increase the global rigidity of the material, preventing some movement of chains in the mobile amorphous phase. So, even if only the mobile amorphous fraction contributes to the glass transition temperature, the RAF content and the crystalline layers near the MAF can shift the T_g to higher temperatures. To sum up, three parameters were reported to influence the amorphous chain mobility: the amorphous/crystalline layers thickness and the RAF content in the crystalline three-phase model.

In all of the papers described above, the crystalline structure modifications were induced by specific thermal treatments. To our knowledge, no nano-structural evolutions were studied after chemical modifications and correlated to the glass transition temperature.

To that extent, the main objective of this work is to study and highlight the structural parameters responsible for the observed T_g shift after chemical modifications of polyamide-6. A classical PA-6 was chemically modified using a small amount of trietheramine. The first part of this paper deals with the chemical mechanism elucidation by liquid NMR and mass spectrometry. Then, the second focus is a study of the resulting changes in the amorphous phase mobility. To finish, a fundamental comprehensive structure-properties relationship is proposed through a study of the degree of crystallinity, crystalline and amorphous lamellae thicknesses, crystalline phases, and spherulites size. In order to do that, AFM, SAXS and WAXS are complementary techniques providing evidence from micrometre to angstrom scale.

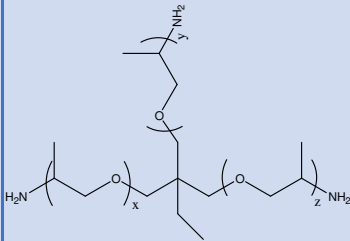
I.2. Materials and formulations

I.2.1. Materials

The matrix polyamide-6 (PA-6) Akulon F136DH[®] was kindly supplied by DSM as polymer pellets. The number-average molar mass was found to be 51 000 g.mol⁻¹ by using size exclusion chromatography in hexafluoroisopropanol (HFIP) and with poly(methyl methacrylate) (PMMA) as a standard. Chain end-group titration on PA-6 gave the real molar mass at 30 770 g.mol⁻¹. The melting point for PA-6 was measured at 219 °C and the degradation temperature at 445 °C by using DSC and thermo gravimetric analysis (TGA) respectively. It was characterized by liquid ¹H and ¹³C NMR (Supplementary file 1) in HFIP/CDCl₃ (80/20 : v/v).

The triamine which is a polyetheramine named T-403 is produced by Huntsman and was directly supplied by Hutchinson Research Center. The chemical structure and number-average molar mass were determined by liquid ¹H and ¹³C NMR (Supplementary file 2) analyses in CDCl₃. The reagent T-403 is a commercial and impurified product which justifies the complexity of the NMR spectra (numerous multiplets).

Table 1: Characteristics of the polyether triamine used with PA-6 (single fitting image)

Structuring agent	Chemical structure	x+y+z (degree of polymerization) ^(a)	M _n (g.mol ⁻¹) ^(a)
T-403		5.10	427

^(a) Average values obtained by ¹H NMR in CDCl₃ and MALDI-ToF MS analyses

Model molecules were used to elucidate the chemical mechanism occurring between PA-6 and T-403 in the extruder. To mimic both the acid and amino polyamide terminal functions, 6-(6-aminohexanoylamino)hexanoic acid was chosen. It was supplied by Angene Company in powder form. Its molar mass is given at 244 g.mol^{-1} . The 1,6-hexamethylenebis(hexanamide) was synthesized to study the reactivity of the PA-6 amide groups. The synthesis protocol and the NMR characterization of the model molecule are detailed in Supplementary file 3.

1.2.2. Sample preparation

Polyamide-6 pellets were first dried under vacuum for 24 h at 80°C to remove water prior to use. Formulations were carried out by melt blending in a co-rotating twin-screw extruder (Leistritz LSM model, $L/D = 34$, $D = 34 \text{ mm}$) at 245°C . In order to ensure sufficient shearing during the process, the screw has two reverse conveying elements. The detailed screw profile is presented Figure 1.

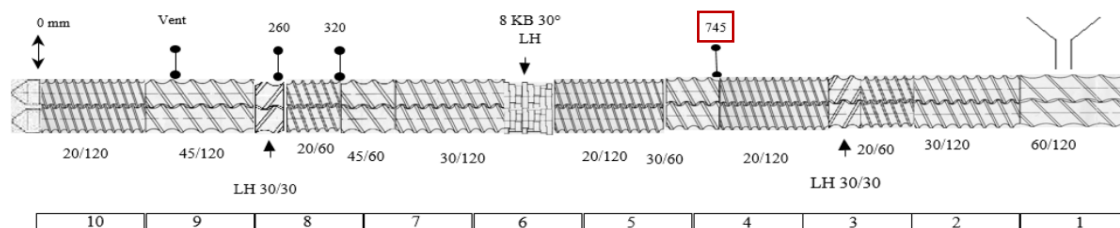


Figure 1: Twin-screw profile with two reverses conveying elements used for the experiment (2-fitting image)

The matrix was incorporated by the hopper at a fixed flow (3 kg.h^{-1}). The reagent T-403 was heated at 50°C to reduce the viscosity and then was added into the matrix in the molten state at the injection point 745 at different flow rates with an external liquid pump. Flow rates were adjusted to incorporate 0.7, 2, 5 and 10 wt% of the structural agent T-403 in the matrix as detailed in Table 2. Screw speed was maintained at 200 rpm. At the end of the extruder, samples were cooled down with air and granulated. The residence time was estimated at approximately 90 s.

Table 2: Molar concentrations for the different reactive blends PA-6/T-403 (mol.kg^{-1} of blend) (single fitting image)

Reactive blends	T-403 (wt%)	$[\text{NH}_2]_{\text{added}}$	$[\text{COOH}]_{\text{polyamide}}$	$\frac{[\text{NH}_2]_{\text{added}}}{[\text{COOH}]_{\text{polyamide}}}$
Polyamide-6/T-403	0.7	0.050	0.032	Excess
	2	0.140	0.032	Excess
	5	0.350	0.031	Excess

	10	0.700	0.029	Excess
--	----	-------	-------	--------

1.2.3. Model medium preparation

Direct NMR analysis of the extruded formulations (polyamide-6/triamine T-403) was not possible because of the poor solubility and the complexity of the reactive medium. In this way, one strategy was to extract the non-reactive triamine and soluble molecules using a Soxhlet extraction in ethanol at 110 °C for 72 h. The fraction isolated after evaporation of the ethanol was analysed by NMR and compared with a fraction obtained after treatment of the pure extruded polyamide under the same conditions. The aim was to identify potential new structures created during the extrusion process. The other strategy was to use several model molecules in order to understand the reactivity of the T-403 on polyamide functional groups. The 1,6-hexamethylenebis (hexanamide) (Figure 3) was selected to mimic the amide functions of the polymer. The protocol of its synthesis is described in Supplementary file 3.

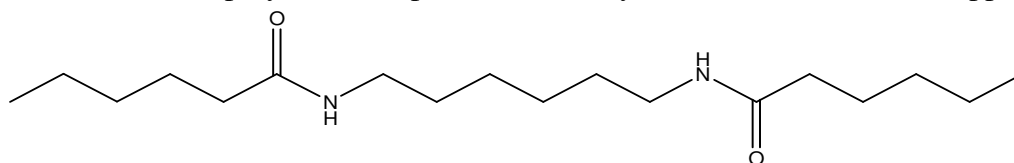


Figure 2: Chemical structure of the hexamethylenebis(hexanamide) (HMDA) (single fitting image)

Besides, the polyamide matrix was modelled using the 6-(6-aminohexanoylamino)hexanoic acid with one amide function and terminated with an amine on one side and a carboxylic acid group on the other side (Figure 3). This molecule was analysed by ^1H and ^{13}C NMR in HFIP/ CDCl_3 (Supplementary file 4). It is called polyamide model or PA model in the text.

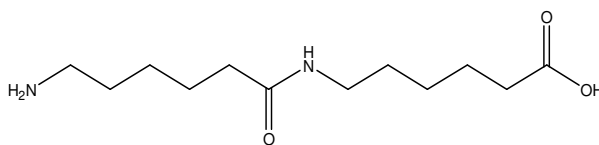


Figure 3: Chemical structure of the 6-(6-aminohexanoylamino) hexanoic acid (polyamide model) (single fitting image)

To use a small quantity of product, a mini reactor in glass flushed with argon was used. Each model molecule [HMDA and 6-(6-aminohexanoylamino)hexanoic acid] was blended in equimolar quantities with T-403 to study the reactivity of amide, carboxylic acid and amine functions with the amino groups of the reagent T-403. The reactions were carried out for 15 minutes at 245 °C. Reaction media were analysed by NMR and new structures were discussed.

I.3. Methods of characterization

Liquid NMR

^1H Liquid-state NMR and diffusion-ordered spectroscopy (DOSY) analyses were performed on a Bruker Avance III spectrometer working at 400.1 MHz with a 5 mm BBFO + probe. A Bruker Avance II spectrometer equipped with a 10 mm ^{13}C selective probe (100.6 MHz for ^{13}C) was used to record 1D- ^{13}C , 2D- $^1\text{H}/^{13}\text{C}$ HMBC and HSQC spectra.

The reagent T-403 was identified in CDCl_3 while formulations (polyamide-6/T-403 Soxhlet extracted fraction) and model reactions were analysed in DMSO at 100 °C and in HFIP- d^2/CDCl_3 (80/20 : v/v) at 25 °C with a concentration of 40 mg.mL^{-1} for ^1H spectra and 110 mg.mL^{-1} for ^{13}C and 2D analysis.

The chemical shift scale was referenced with tetramethylsilane used as internal standard to calibrate the spectra at 0 ppm.

2D ^1H -DOSY experiments were implemented using the double stimulated echo sequence with bipolar gradient pulse (dste-bp). Samples were analysed in a mixture of HFIP- d^2/CDCl_3 (80:20 v/v) with a concentration at 20 mg.mL^{-1} . Before each experiment in DOSY, diffusion time (d20) and gradient duration (p30) was adjusted to study the exponential decrease of the peak intensity as a function of the gradient (from 0.96 G.cm^{-1} to 47187 G.cm^{-1}). Data analysis was performed on Topspin 3.5 software.

Mass spectrometry by MALDI-ToF

MALDI-ToF MS analyses could not be realized on the extruded formulation and Soxhlet extracted fractions because of high molar mass species and the resulting ion detection deficiency. The product of the reaction between the polyamide model and T-403 was solubilized in HFIP (10 g.L^{-1}). Dithranol, as a matrix, was added to the solvent at 10 g.L^{-1} . Then, 1 μL of the sample was mixed with 9 μL of the matrix. This mixture was spotted onto a MALDI plate and air-dried to vaporize the solvent and co-crystallize the sample and the matrix. Desorption and ionization with the laser produced protonated ions. The polyamide model and the reactant T-403 alone were analysed as references. The analyses were carried out with a Voyager-DE STR (AB Sciex, Framingham, MA) at a tension of 20 kV. The positive mode is preferred because molecules of the analyte are easily protonated. Both linear and reflection modes were implemented.

Thermal analysis: Differential Scanning Calorimetry (DSC)

Thermal properties of the formulations were characterized by DSC in order to study the melting and crystallization behaviour using the model Q2000 (TA Instruments) equipped with a refrigerated cooling system 90. Indium was used as calibration standard. Before analysis, samples were dried under vacuum at 80 °C for 24 h. Then, 5 to 10 mg of the

dumbbell specimen (for tensile test) was weighed and placed in a hermetic aluminium capsule. The value of the melting temperature (T_m), crystallization temperature (T_c) and enthalpy were measured on the first cycle applied from 20 °C to 250 °C at a heating rate of 10 °C.min⁻¹. The degree of crystallinity was calculated with the equation as follows:

$$\chi_c = \frac{\Delta H_m}{\Delta H_m^0} \quad (1)$$

where ΔH_m is the sample melting enthalpy and ΔH_m^0 is the melting enthalpy of 100% crystalline PA-6 ($\Delta H_{mPA-6}^0 = 190 \text{ J.g}^{-1}$) [31].

Modulated DSC (MDSC) was implemented to measure the glass transition temperature (T_g) of the different blends because, as for polyamide-6, the heat capacity step ΔC_p (used to measure the T_g) is quite wide and weak. Approximately 15 mg of the samples were introduced in a hermetic aluminium pan. It should be noted that the samples were dried carefully because water absorption led to a significant decrease of the T_g and non-reproducible results. The temperature was equilibrated at - 20 °C and then increased up to 140 °C with a heating rate of 2 °C.min⁻¹ with a temperature modulation of ± 4 °C every 60 s. In our case, the T_g value is the midpoint of the step observed in the DSC curve and given by the TA Universal Analysis software.

The analyses were carried out on dumbbell specimens (shaped H2) made with a hydraulic injection moulding machine Babyplast 6/10P equipped with a piston diameter of 14 mm and presenting a clamping force of 62 kN. Chamber temperature was set at 260 °C, mould temperature at 80 °C, and the injection pressure at 70 bar.

Atomic Force Microscopy (AFM)

Tapping mode AFM images were obtained with a Nano-observer from CSI in order to compare the topography and the spherulite size of the different formulations under ambient conditions. Samples were previously microtomed with a diamond knife at - 120 °C to obtain a roughness below 20 nm. The surface quality was checked by optical microscopy before analysing.

Size Exclusion Chromatography (SEC)

The molar mass of the different formulations were determined by SEC Acquity advanced chromatography from Waters with a RI detector (Agilent-RI-1100). Three columns were used: Apc XT 450, 125 and 45. HFIP was the eluent at a flow rate of 0.3 ml.min⁻¹. Samples (around 10 mg) were first solubilized for several hours in 1 mL of HFIP and filtered. Approximately 20 μ L was injected into the column. The average molar masses M_n and M_w were determined with a calibration method using polymethyl methacrylate (PMMA) standards.

Dynamic Mechanical Analysis (DMA)

A DMA Q800 from TA Instruments was used in tension to investigate the dynamic mechanical properties of formulations. Rectangular samples with dimension 25 mm × 7 mm × 1 mm prepared by compression moulding at 260 °C were fixed vertically between clamps, and dynamic temperature sweeps were performed from -100 to 200 °C at fixed frequencies (3, 5, 10, 30 and 50 Hz) and at a heating rate of 2 °C.min⁻¹. The samples were dried at 80 °C under vacuum for 24 h and then stored in desiccators until measurements were made. The storage modulus (E') and loss tangent ($\tan \delta$) were measured as a function of temperature for all of the specimens under the same conditions.

X-ray diffraction: Wide Angle X-ray Scattering (WAXS) and Small Angle X-ray Scattering (SAXS)

X-ray scattering analysis on polyamide-6 is a non-destructive powerful technique to study its crystallinity (orientation, phase, size, and shape).

The measurements were carried out at the European Synchrotron Radiation Facility (ESRF) in Grenoble on the BM2-D2AM beamline. The incident photon energy was set at 16 keV and two detectors were used for SAXS (D5) and WAXS (WOS) analyses. The sample-to-detector distance was about 1.15 m SAXS and 11.0 m WAXS and the beam stop had a diameter of 1 mm. The q-range calibration was made with a silver behenate (SAXS) and lanthanum hexaboride (WAXS) as standards. The two-dimensional data were corrected by considering the camera geometry, dark image reading, and flat field response of the detector. Each sample was put in Kapton tape and placed at the centre of the sample holder. The value obtained for the empty cell with Kapton tape was subtracted from the scattering images of the studied sample.

The measurements were carried out on dumbbell specimens (shaped H2) made as described for the DSC analyses. A bench type press Polystat 200 T (Servitec) at 260 °C was used to make films of the blends without any preferential orientation.

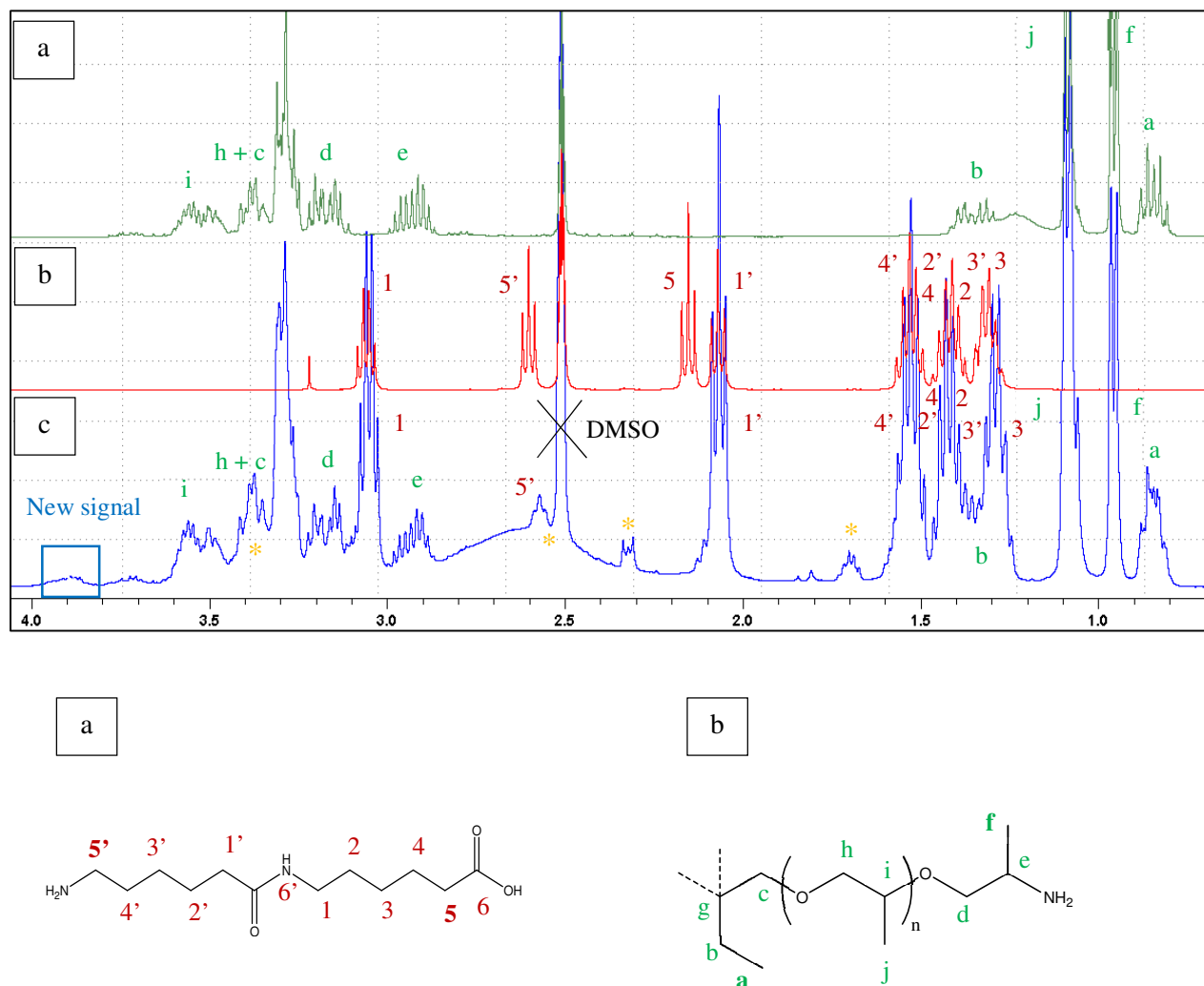
1.4. Results and discussion

As detailed previously, four concentrations of the reagent T-403 were added to polyamide-6 using a twin-screw extruder. In order to study the influence of the new chemical structures on the amorphous phase mobility, a certain number of experiments were carried out. In a first part, the results of liquid NMR and MALDI-ToF MS are analysed in order to highlight the chemical mechanism occurring during the extrusion process. Then, the chain mobility in the amorphous phase was linked to the crystalline morphology brought about by the new complex structures synthesized.

1.4.1. Chemical mechanisms

a. Evidence of a reaction between carboxylic acid end-groups and the reagent T-403

The ^1H , ^{13}C and 2D NMR spectra were analysed to look for evidence of the formation of new structures between the reagent T-403 and the polyamide model. First, the ^1H NMR spectra of the reagent T-403, the polyamide-6 model molecule and the reaction medium (after 15 minutes at 245 °C) in DMSO at 100 °C are compared for different NMR zones in Figure 4 and Figure 5.



**: Caprolactam produced by transamidification of polyamide model*

Figure 4: ^1H NMR spectra between 0 and 4 ppm of: (a) T-403, (b) polyamide model and (c) reactional medium in DMSO at 100 °C and after 15 minutes at 245 °C (“keep colors”) (2 fitting image)

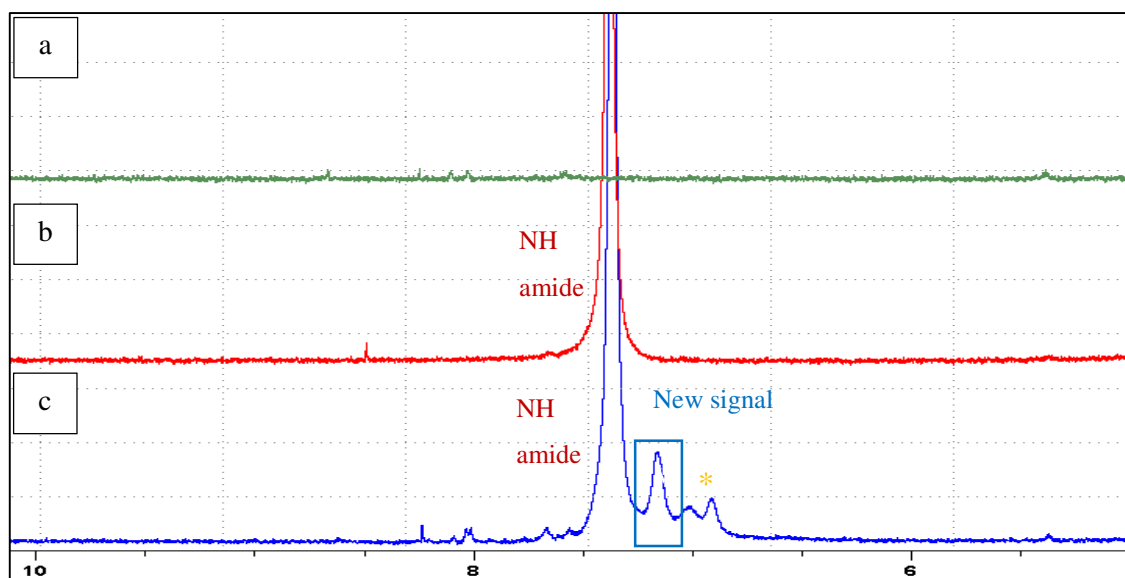


Figure 5: ^1H NMR spectra between 5 and 10 ppm of: (a) T-403, (b) polyamide model and (c) reactional medium in DMSO at 100 °C and after 15 minutes at 245 °C (“keep colors”) (2 fitting image)

By comparing these spectra, new interesting signals can be observed at 3.92 ppm and around 7 ppm. The signal at 3.92 ppm (CH area) was correlated in 2D-HSQC spectra at 45 ppm and in 2D-COSY and TOCSY spectra at 7.14, 1.07 (CH₃ near the new amide function) and 3.38 ppm. This signal belongs to the CH zone and may be a group of the modified reactant T-403. The 2D correlation gave the neighbour groups depicted in Figure 6.

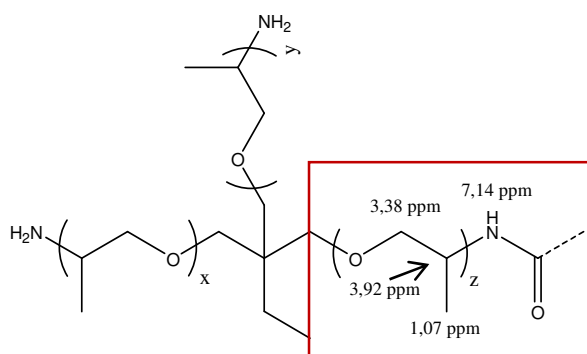


Figure 6: Structure created after the reaction of the reagent T-403 amino group and polyamide-6 model (single fitting image)

By integration of the area of the signals 5 and 5' after reaction and taking the signal **a** of T-403 as a reference, carboxylic acid was converted by 71 mol% and the amine function by 55 mol% which means that a part of the -COOH functions were consumed by a reaction. This observation was confirmed by the disappearance of the carboxylic acid peak on the ^{13}C spectra. Thanks to the good definition of the ^1H spectra in DMSO, the area of the signal **f** was

integrated before and after the reaction. The area decreased from 6.04 to 4.93. As a result, less than 20 mol% of the structural agent T-403 reacts on the polyamide model.

Two side reactions were also identified. The predominant reaction is the polycondensation of the model molecule alone leading to chain lengthening. The major consequence of this reaction on the ^1H NMR spectrum was the important lowering of the intensity of the signal 5 and 5'. The second reaction is the cyclisation (Figure 7) of the model molecule and the formation of caprolactam with characteristics signals at 1.7, 2.5, 2.8, 3.4 and 7 ppm. These side reactions can potentially decrease the efficiency of the reaction between T-403 and the PA model.

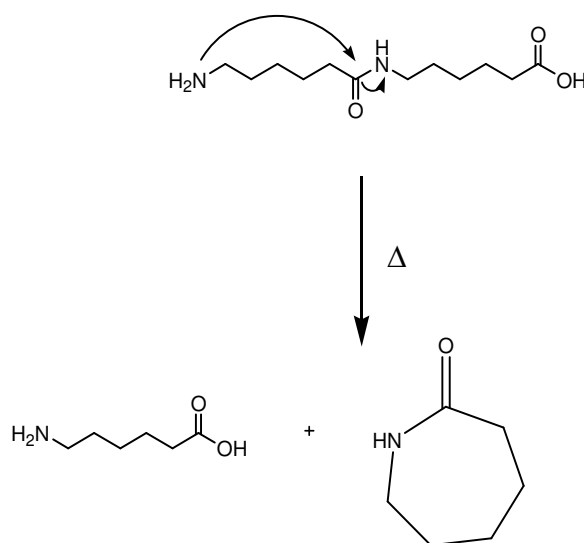
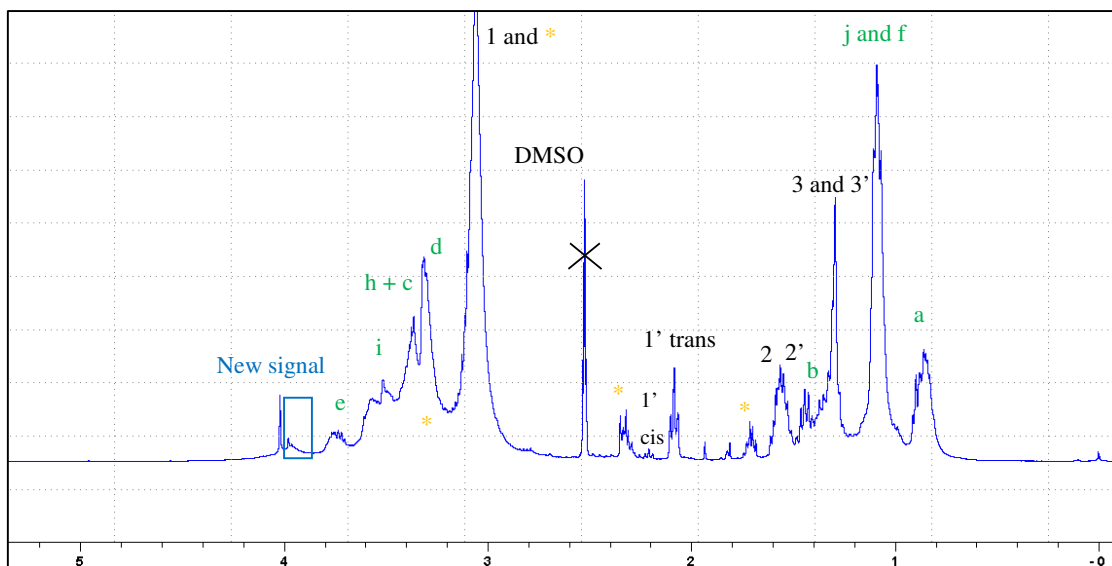


Figure 7: Cyclization mechanism of polyamide model (single fitting image)

To be more representative of the medium obtained in the extruder, ^1H (Figure 8) and ^{13}C NMR analyses (Supplementary file 5) of Soxhlet extracted fractions from the reaction between polyamide-6 and T-403 (10 wt% of T-403) were realized. These latter fractions were directly compared to those obtained from virgin and extruded polyamide-6 alone. In both spectra, we noticed the apparition of new amide functions at around 7-8 ppm and 175-180 ppm, respectively. Again, a new interesting peak was observed at 3.98 ppm and 2D correlation gave the same neighbour groups as the one represented in Figure 6.



*: Caprolactam extracted during the Soxhlet extraction

Figure 8: ^1H NMR spectrum between 0 and 5 ppm of polyamide-6/reagent T-403 Soxhlet extracted fraction in DMSO at 100 °C after reactive extrusion (“keep colors”) (2 fitting image)

To confirm the presence of new species resulting from the grafting of T-403 on polyamide-6, DOSY analyses were performed on the model reaction media before and after reaction. This Pulse Field-Gradient NMR technique, based on translational diffusion measurements, is used to separate species of a mixture according to their molar mass and specific architectures. During DOSY experiments, in addition to the routinely used radio-frequency pulses, magnetic field gradient pulses are applied to get spatial information.

NMR spectra were obtained for several values of gradient strength (g) while keeping constant other gradient parameters, and diffusion coefficients were determined by fitting the signal attenuation given by the Stejskal-Tanner equation [33]:

$$I = I_0 \cdot \exp(-D(\gamma\delta g)^2 \cdot (\Delta' - \frac{\delta}{3} - \frac{\tau}{3})) \quad (2)$$

where I is the attenuated intensity of a signal at a frequency, I_0 is the reference intensity of the same signal with $g = 0$, D is the self-diffusion coefficient, γ is the gyromagnetic constant of the hydrogen nucleus, δ is the gradient pulse length, and Δ' is the corrected value of Δ which depends on the specific pulse sequence used and the gradient shape. By plotting $\ln(I/I_0)$ versus g^2 (see equation 2), one straight line should be obtained with a slope proportional to the diffusion coefficient for a single monodispersed component.

By contrast, if the curve is a non-linear decay, the studied signal could result from a mixture of several components or a polydispersed moiety such as polymers [34, 35].

DOSY measurements were realized on the model reaction medium and the $-\text{CH}_3$ signal (**a**) of the reagent T-403 was chosen to follow the attenuation as a function of the gradient strength. As a reference, the same experiment was implemented on the non-reacted medium of PA model and T-403 using the same ratio, concentration, and conditions (temperature and other parameters). Both resulting curves are represented in Figure 9.

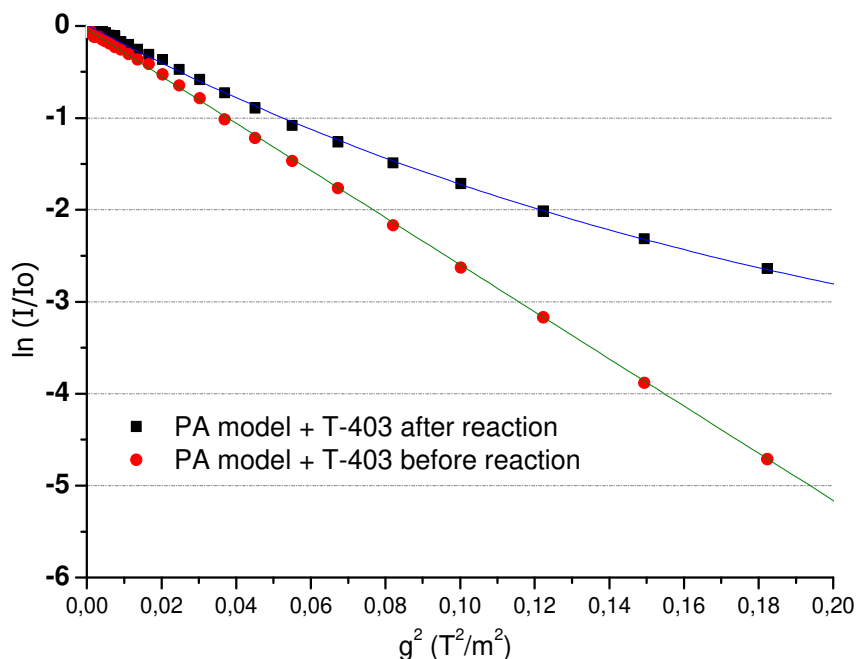


Figure 9: Logarithm of the normalized signal attenuation versus the square root of gradient strength for the signals (**a**) in the model medium before and after reaction (“keep colors”) (single fitting image)

The curve decay for the solvent HFIP- d^2 (not shown here) was linear in both media (before and after the reaction) and approximately the same diffusion coefficient was found. For the non-reacted sample, the curve could have been fitted by one linear function. Despite the polydispersity (between 4 and 8) of the T-403 calculated by MALDI-ToF MS, it can be considered as a single molecule with a unique molar mass regarding its diffusion through DOSY experiments. After the reaction, the curve decay presents a clear deviation from the linear tendency previously observed. This observation is important because it reflects a noticeable modification of the reagent T-403 after reaction, as different diffusion coefficients can be calculated (larger polydispersity). This observation allowed us to confirm that the T-403 reagent is modified through the reaction with the PA model after 15 min at 245 °C. The DOSY experiments seem to confirm the reaction between the model of polyamide and the reagent T-403 as demonstrated by ^1H and ^{13}C NMR analyses.

Finally, MALDI-ToF MS analyses were carried out on the reaction medium between polyamide model/T-403. Two populations were observed at low and high m/z . Low m/z was

assigned to the triamine T-403 and the DP was found to be between 4 and 8 in accordance with the liquid NMR analyses. Among the high m/z , many signals were attributed to new compounds resulting from the reaction of the reagent T-403 on the polyamide model. Some of these compounds are listed in the Table 3 and an example of a structure created is represented Figure 10.

Table 3: Products of reaction (amidification) between the polyamide model and T-403 analyzed by MALDI-ToF MS (single fitting image)

DP (x + y + z)	Number of reacted polyamide model	Chemical formula $M + Na^+$	Experimental $M + Na^+$ (m/z)
6	3	$C_{60}H_{119}O_{12}N_9Na$	1180.89
7	3	$C_{63}H_{125}O_{13}N_9Na$	1238.93
8	3	$C_{66}H_{131}O_{14}N_9Na$	1296.97
5	4	$C_{69}H_{135}O_{13}N_{11}Na$	1349.01
6	4	$C_{72}H_{141}O_{14}N_{14}Na$	1449.06

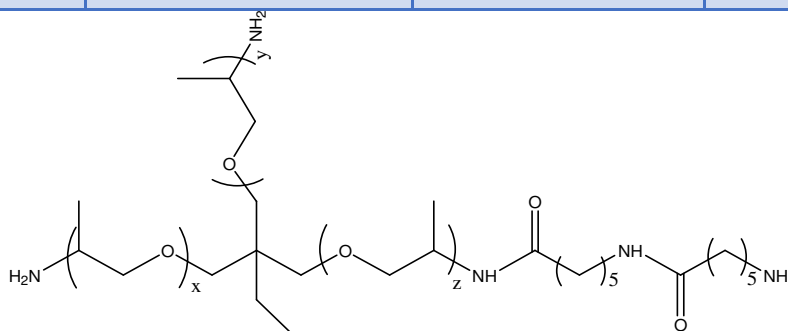


Figure 10: Example of structure resulting from the reaction of the reagent T-403 on the polyamide model through the -COOH function (single fitting image)

The results obtained by MALDI-ToF mass spectrometry confirm the hypothesis of a grafting reaction between polyamide-6 carboxylic acid end-groups and the structural agent T-403. Nevertheless, the determination of the exact structure created is difficult because of the contribution from side reactions such as condensation reactions. Thus, polyamide-6 model can

react with one or several amino groups of T-403 and potentially develop a star-shaped structure [32].

b. Evidence of the reaction between amide and amine groups of the reagent T-403

Furthermore, in order to study the reactivity of a primary amine toward an amide function, HMDA was mixed with an equimolar quantity of T-403 for 15 minutes at 245 °C in the mini reactor under argon atmosphere. ^1H NMR analysis of the reaction medium was realized in DMSO at 100 °C (Figure 11). Once more, we noticed the presence of a new small signal at 3.90 ppm that is similar to that obtained from the Soxhlet extracted fractions and the reaction between polyamide-6 model/T-403. Another evidence of the transamidification reaction was the reduction of the signals near the amine of the T-403 and the disappearance of 12% of the HMDA amide functions. New amide functions (resulting from the transamidification) were noticeable at 7.16 and 7.68 ppm.

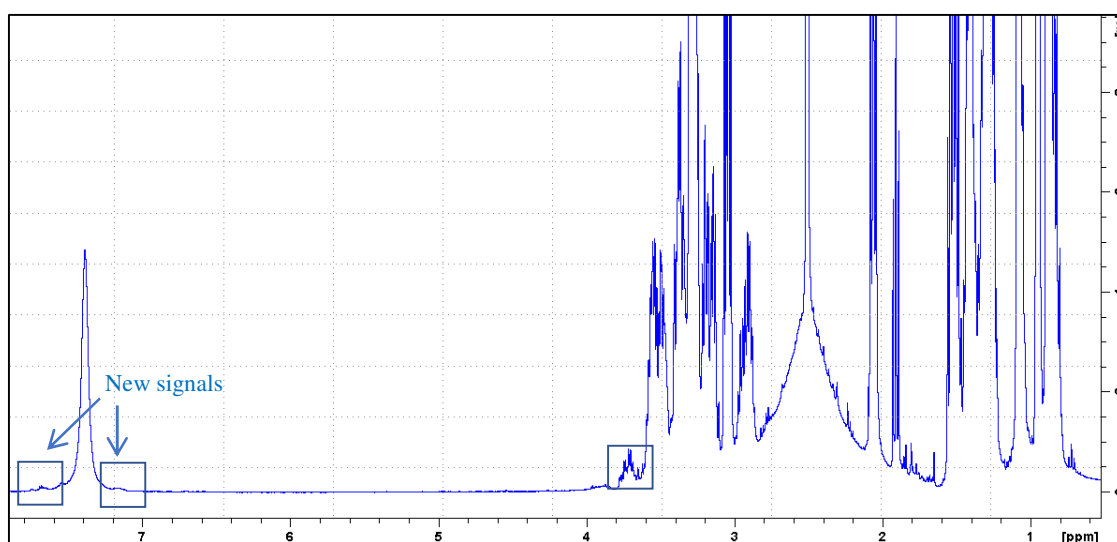


Figure 11 : ^1H NMR spectrum in DMSO at 100 °C (0 and 8 ppm) of the reaction medium after reaction at 245 °C/15 min between HMDA and T-403(single fitting image)

This reaction between the amino groups of T-403 and the amide functions of HMDA should lead to chain scissions. This latter reaction was highlighted by SEC analyses on the four samples obtained after reactive extrusion between PA-6 and T-403. The number-average molar mass was found to decrease with the addition of T-403. For example, the M_n varied from 51 000 g.mol⁻¹ for polyamide-6 to 44 000 g.mol⁻¹ for the blend with 2 wt% of T-403. MALDI-ToF MS analyses were again applied to the reaction medium between the polyamide model and T-403. These results confirmed that transamidification can occur during the reaction. However, it is worth mentioning that the m/z values listed in Table 4 could also be attributed to a reaction between the triamine T-403 and the 6-aminohexanoic acid molecule synthesized by cyclization of the polyamide model depicted in Figure 7.

Table 4: Products of reaction (transamidification) between the polyamide model and the reagent T-403 analyzed by MALDI-ToF MS (single fitting image)

DP (x + y + z)	Number of grafted polyamide model	Chemical formula M + Na ⁺	Experimental M + Na ⁺ (m/z)
4	4.5	C ₇₂ H ₁₄₀ O ₁₃ N ₁₂ Na	1404.06
4	2.5	C ₄₈ H ₉₆ O ₉ N ₈ Na	951.72
4	3.5	C ₆₀ H ₁₁₈ O ₁₁ N ₁₀ Na	1177.89
4	5.5	C ₈₄ H ₁₆₂ O ₁₅ N ₁₄ Na	1630.22
5	2.5	C ₅₁ H ₁₀₂ O ₁₀ N ₈ Na	1009.76

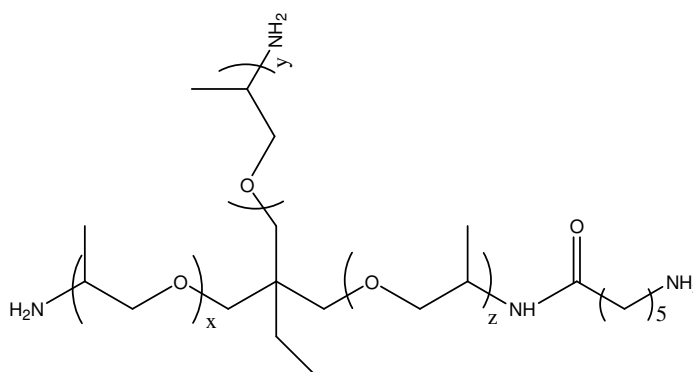


Figure 12: Example of structure resulting from the transamidification between the reagent T-403 and the polyamide model (single fitting image)

c. Chemical mechanisms for the reaction between PA-6 and the reagent T-403

Based on the previous analysis on the models compounds reaction media, it is clearly observed that the polyetheramine T-403 can react on the polyamide carboxylic acid end-groups or on amide. Thus transposed to the polymer medium treated in the same range of temperature, a chemical mechanism of the reaction between polyamide-6 and the reactant T-403 can be proposed (Figure 13). Transamidification and amidification will lead to branched and linear chains during reactive extrusion of the polyamide 6 and the T-403 reagent.

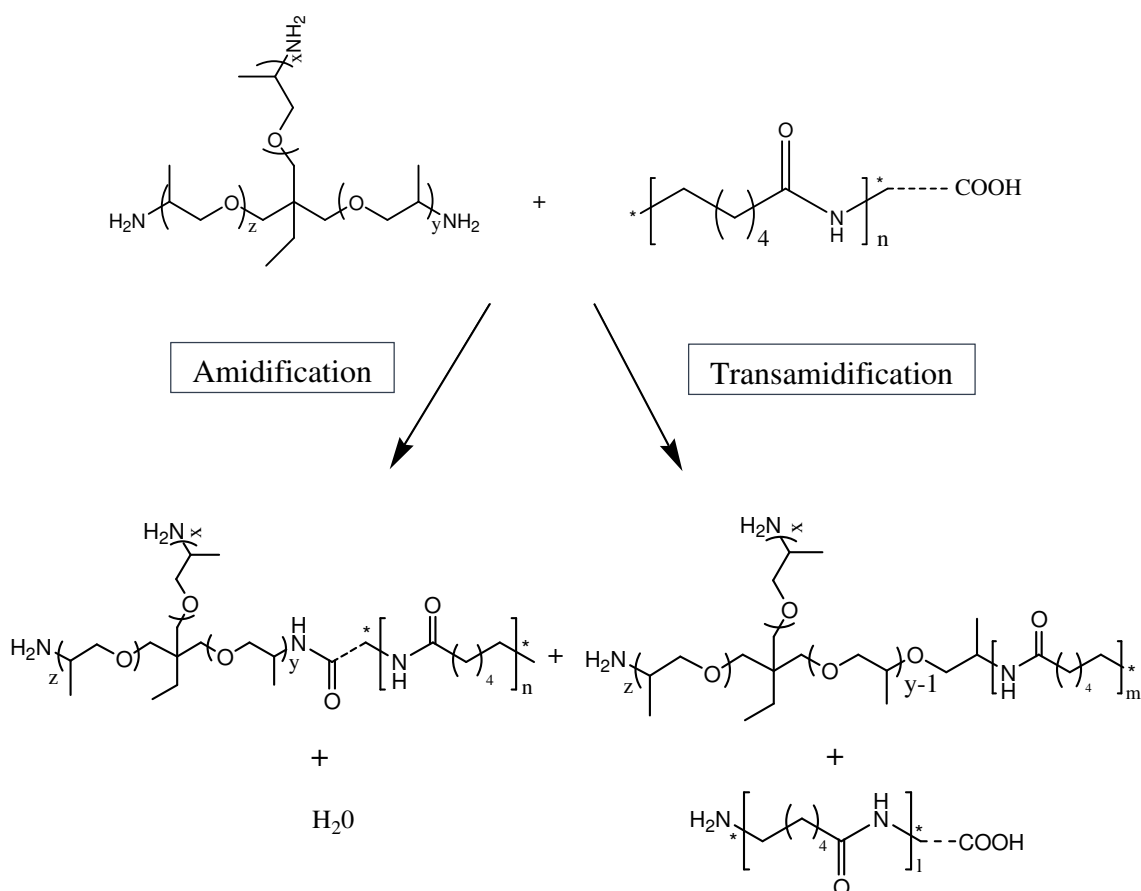


Figure 13: Reaction scheme of the polyamide-6 repeating with the reagent T-403(1.5 fitting image)

1.4.2. Structure/amorphous phase mobility relationship

It has been demonstrated in part II.4.1) that the addition of T-403 induced a chemical modification of polyamide-6. The purpose of this second part is to evaluate the impact of the new structures synthesized on the amorphous phase mobility. This latter modification is then interpreted via a detailed investigation of the small scale morphology of the matrix, as for example the degree of crystallinity, but also the amorphous/crystalline lamellar thicknesses and composition. In order to study such evolution, modulated DSC, DMA, AFM and SAXS-WAXS experiments were conducted on polyamide-6/T-403 blends.

a. Chain mobility in the amorphous phase of the PA-6/T-403 reactive blends

Chemical modifications of polymers could induce amorphous phase mobility (T_g) variations. In a recent study, A. Rios De Anda et al. [36] studied molecular mobility of chemically modified polyamide-66 in which aromatic rings were introduced in the aliphatic backbones. The resulting copolymers were synthesized by polycondensation between 95 mol% of adipic acid and 5 mol% of either isophthalic acid-based phenol (HIA) or isophthalic acid-based lithium salt (AISLi) with hexamethylene diamines. Both DSC and DMA analyses

demonstrated that the addition of rigid groups restricts the chain mobility. This lower mobility induced higher T_g values at 77 °C for the copolymer PA-6,6/HIA and 91 °C for the PA-6,6/AISLi instead of 71 °C for the unmodified polyamide-6,6.

In order to study more specifically the influence of the new branched structures on the amorphous phase behaviour, DMA and modulated DSC measurements were realized.

According to the modulated DSC results, summed up in the Table 5, the glass transition temperature was higher for 0.7 wt% of T-403 added (59.3 °C), constant for 2 wt% (52.0 °C) and lower for 5 wt% (48.8 °C) and 10 wt% of T-403 added respectively compared to the value obtained for the virgin PA-6. A higher T_g expresses a decrease of mobility in the amorphous phase of the material. In the literature, a higher glass transition temperature can be related to free volume reduction [37-39], a more rigid group added into the polymer chain (aromatic group) [40], or specific crystalline morphology (higher RAF content, thinner amorphous phase lamellae...) [28-30]. Over 2 wt%, the unreacted T-403 molecules accumulated in the polymer and this lead to a significant decrease of the T_g values. The T_g lowering is often a good proof of plasticization behaviour. Indeed, the addition of small molecules breaks the well-ordered networks of interchain hydrogen bonds at some point promoting chain movement. In addition, the free amine groups of the T-403 are able to create intramolecular H-bonds. Besides decreasing the T_g value, the easier segment motions often reduce the T_f, T_c, viscosity, yield strength and Young's modulus while increasing the elongation at break [39-41].

These physico-chemical property modifications were confirmed by Belous et al. [37] in their study about the plasticization efficiency of several additives in polyamide-6. By addition of 10 wt% of benzene surfonamide (BSA), the T_g decreased from 62 to 46 °C, the T_f from 223 to 215 °C and the T_c from 187 to 181 °C. The plasticized material exhibited a lower tensile resistance with a decrease of the Young's modulus and the yield strength by 200 MPa and 5 MPa, respectively. The elongation at break was increased by approximately 40%.

Table 5: Glass transition temperatures obtained for the reactive blends PA-6/T-403 (modulated DSC) (single fitting image)

Formulations	T _g (°C)
Extruded PA-6	52.0 ± 0.5
PA-6/T-403 0.7 wt%	<u>59.3 ± 0.4</u>
PA-6/T-403 2 wt%	52.1 ± 0.5
PA-6/T-403 5 wt%	48.8 ± 0.3
PA-6/T-403 10 wt%	/

Chain mobility was also studied using DMA. The evolution of $\tan \delta$ versus temperature for polyamide-6 revealed three peaks. Two of them are associated to sub-glass transitions and one is associated to the glass transition. The first secondary relaxation is the γ -transition located between - 120 and - 110 °C and corresponds to local segmental motions of methylene groups between amide functions. The second is the β -relaxation between - 60 and - 40 °C which is related to the rotation of the amide functions of polyamide-6. Secondary relaxations are associated with the material properties in the glassy state [42]. The primary relaxation called α is attributed to long segmental motions (no less than 15 monomers). Measured at 1 Hz, the T_α can be considered equivalent to the glass transition temperature (T_g).

Both α - and β -transitions in the reactive polyamide-6/T-403 blends were investigated and results are presented in Table 6 and in Figure 14.

Table 6: T_α, T_β and β amplitudes obtained for the reactive blends PA-6/T-403 (DMA at 10 Hz) (single fitting image)

Formulations	T _α	T _β	β amplitude
Extruded PA-6	83.33	- 37.32	0.0137
PA-6/T-403 0.7 wt%	<u>87.87</u>	- 35.20	0.0098
PA-6/T-403 2 wt%	83.46	- 36.58	0.0094
PA-6/T-403 5 wt%	83.09	- 37.79	0.0099
PA-6/T-403 10 wt%	81.73	- 42.14	0.0178

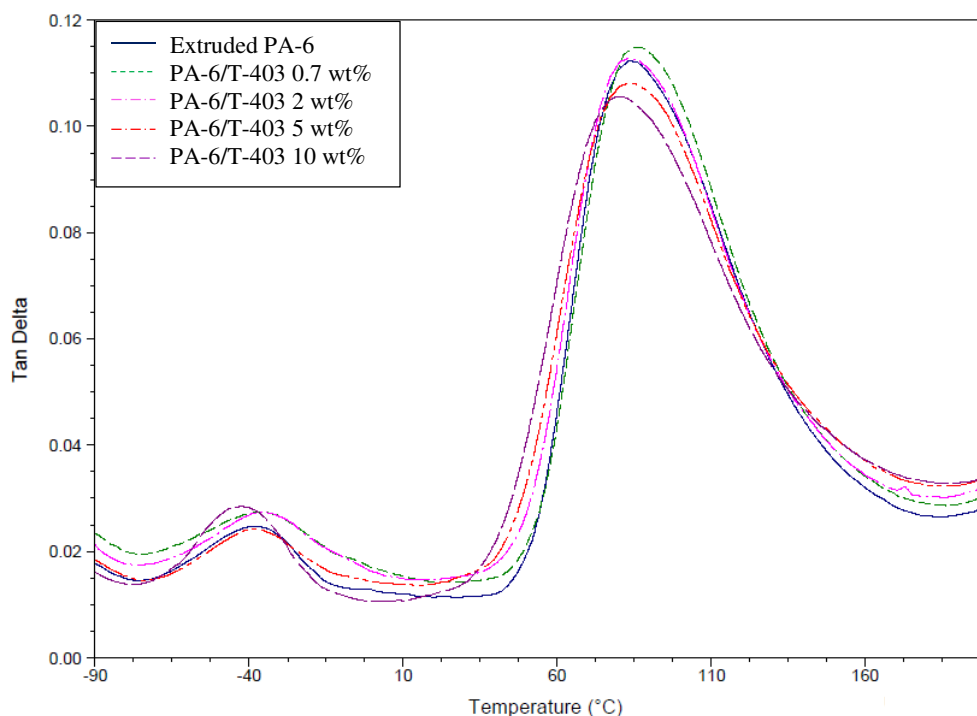


Figure 14: $\tan \delta$ versus temperature obtained by DMA analysis at 10 Hz for the reactive blends PA-6/T-403 (“keep colors”) (single fitting image)

For 5 and 10 wt% of T-403, the results illustrated flattening of the loss angle tangent ($\tan \delta$) and a shift towards lower temperatures of the β -transitions, characteristic of plasticization behaviour (mobility promoted) as observed by DSC [43, 44]. The β -transition intensity depression induced by the addition of plasticizers was detailed by Vilics et al. in a paper about the relaxation behaviour of plasticized PVC. The author defined a good compatibilizer as an additive compatible and able to lower significantly the T_g of the material. Efficient compatibilizers such as phthalate (for PVC) flattens the β -transition and sometimes even suppresses it. Among the numerous plasticizers studied, the di-2-ethylhexyl-phthalate (DEHP) appeared to be an efficient compatibilizer as for 5 wt% added, the β -transition intensity was flattened from 0.03 to 0.02 and the signal was shifted towards lower temperature (- 75 instead of - 60 °C for the pure PVC). For higher concentrations (> 10 wt%), the plasticization effect cannot be properly estimated because of overlapping with the α -transition (important decrease of the T_g value).

The variation of the α -relaxation temperature (T_α) measured by DMA followed the same trend as the T_g obtained by modulated DSC. Indeed, the T_α value increased for the material obtained with 0.7 wt% of T-403, remained constant for 2 wt% of T-403, and then decreased below that of the extruded polyamide at higher T-403 concentrations.

Mobility hindering by addition of small amounts of T-403 was also confirmed with the β -transition. Indeed, for 0.7 and 2 wt% of T-403, we observed a decrease of the β -amplitude meaning that local movements related to the β -relaxation were restricted [24, 44, 45]. To explain the T_g enhancement observed for a small amount of the reagent T-403 (< 2 wt%), the different environments felt by the mobile amorphous phase at the lamellar scale were estimated as the

glass transition involves cooperative motions at nano-metric length scale. With this in mind, the nano-structuration and particularly the crystallinity parameters of the material will be studied at different scales.

b. Micro- and nano-structural morphology evolutions for the PA-6/T-403 reactive blends

A complete study of the polymer crystallinity is sometimes essential to explain the chain mobility evolution. Indeed, it has been reported in articles that the chain orientation, the degree of crystallinity [14], the nature of the crystalline phase [1], the size of the crystallites [46], and the crystalline phase structure [24] could induce geometrical restrictions on local movements and lead to glass transition temperature shifts. The crystalline and amorphous modifications at different scales were studied using four powerful techniques. Thus, DSC and AFM were implemented not only to assess the potential evolution of crystallinity but also to probe the crystallite size and shape. WAXS was used to compare the crystalline phase nature present in the different reactive blends. Finally, SAXS measurements were carried out to obtain the crystalline structure at the smaller scale, that is to say the lamellae thicknesses and composition, crystallinity, and crystallite size

First, the thermal properties and the crystallinity were studied by differential scanning calorimetry. The values obtained for the samples are listed in the Table 7 and the melting/crystallization peaks are presented in Figure 15.

Table 7: Crystallization temperature (T_c), melting temperature (T_m) and degree of crystallinity (χ_c) values obtained for the extruded PA-6 alone and the reactive blends PA-6/T-403 (“keep colors”) (single fitting image)

Formulations	T_c (°C)	T_m (°C)	χ_c (%)
Extruded PA-6	187.9	221.0	32.5 ± 0.2
PA-6/T-403 0.7 wt%	188.0	221.7	35.2 ± 0.7
PA-6/T-403 2 wt%	188.7	221.9	35.0 ± 0.3
PA-6/T-403 5 wt%	190.3	222.1	33.2 ± 1.1
PA-6/T-403 10 wt%	191.2	220.7	30.1 ± 0.7

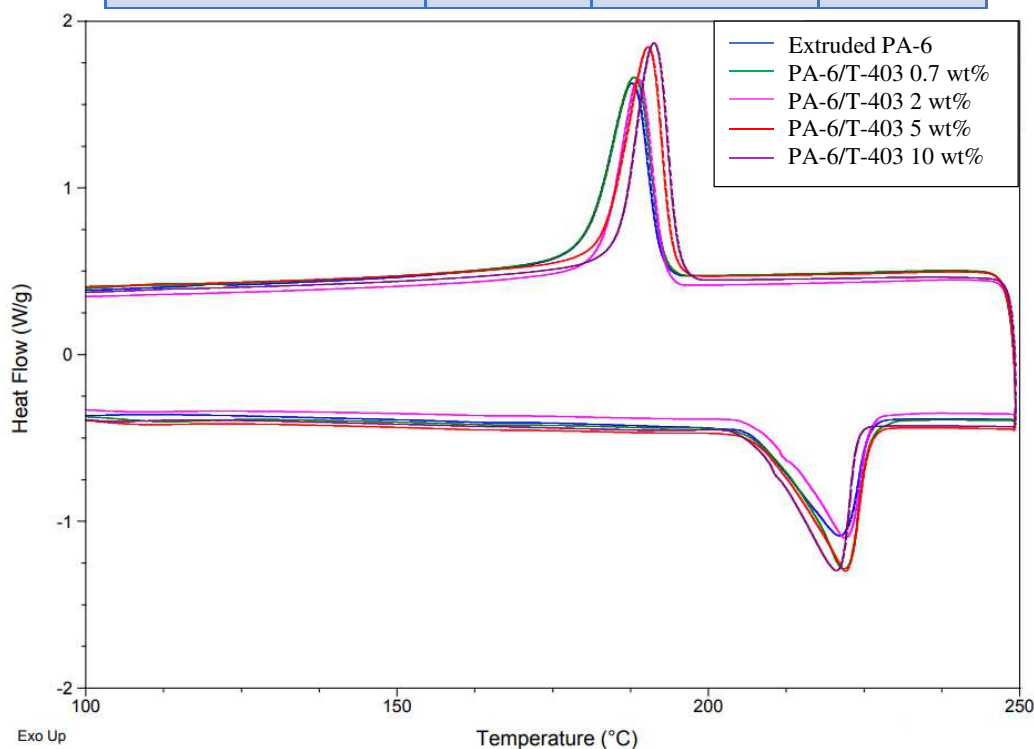


Figure 15: Melting and crystallization zones for the extruded PA-6 alone and the blends PA-6/T-403 (“keep colors”) (single fitting image)

The introduction of T-403 into polyamide-6 resulted in slight thermal property changes. The T_m variations were not significant enough to be considered, while the T_c increased gradually with the addition of T-403, meaning that the crystallization process is promoted by the shorter polymer chains. The width of the melting peaks was comparable, which means that the incorporation of T-403 did not affect the crystal size.

To support this latter observation regarding the crystallite dimensions, AFM analyses were carried out. Microtomed surfaces of extruded polyamide and polyamide modified with 2 wt% of T-403 were studied (Figure 16). AFM topography images ($20 \times 20 \mu\text{m}^2$) were taken to observe several spherulites micro-structures and study the morphology at a larger scale. The average spherulite diameters could be measured and estimated at $2.2 \pm 0.6 \mu\text{m}$ for the virgin polyamide-6 and $2.5 \pm 0.3 \mu\text{m}$ for the sample PA-6 + 2%wt T-403. The T-403 reagent did not induce significant spherulite size modification.

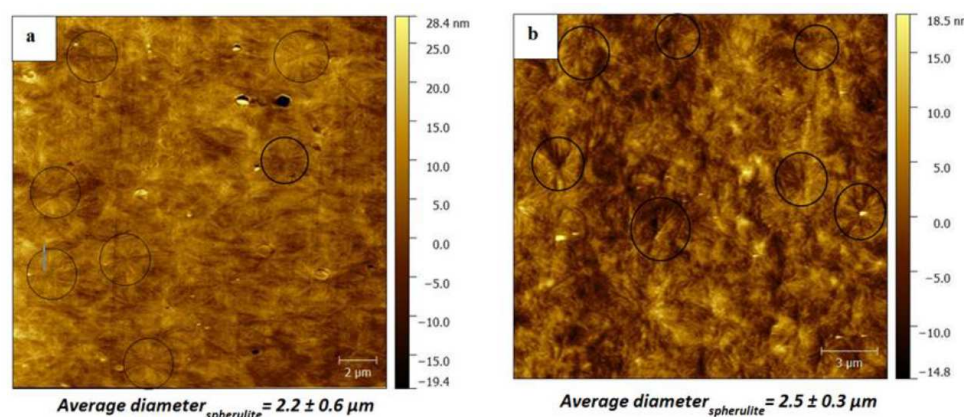


Figure 16: AFM topography images of (a) the extruded PA-6 and (b) the reactive blend PA-6/T-403 2 wt% ("keep colors") (single fitting image)

The crystallinity modification was noteworthy for a small amount of T-403 (≤ 2 wt%). For low T-403 concentrations, the molar mass decrease may explain the higher crystallinity ratio calculated. Shorter polymer chains have better mobility in the molten state and exhibit fewer entanglements per chain, as detailed in the previous part. In addition, small molecules can promote chain mobility and thus increase the degree of crystallinity. This latter point could explain the higher crystalline content measured for the blend PA-6/T-403 0.7 and 2 wt%. Indeed, Li *et al.* [47] succeeded in enhancing the crystallinity degree of their poly(lactic)acid from 14% to 40% by adding 5 wt% of polyethylene glycol and moulding at 80 °C.

For higher concentrations of T-403, the crystalline content decreased below that of the pure PA-6. The crystallization was inhibited due to the plasticization effect of the excess T-403 as discussed before. No noticeable modification was observed regarding the crystallite size and shape at the micro-scale. In the subsequent stage of the study, the goal was to focus on the crystalline phase nature and the structural organization at the nano-scale in the reactive blends.

Crystalline phase nature and lamellar thicknesses

SAXS-WAXS studies were carried out on injected dumbbell specimens made under the same experimental conditions (temperature and pressure). The aim of the WAXS experiments was to identify the crystalline phases present into the materials while the SAXS was used to calculate the lamellar dimension and composition.

For semi-crystalline polymers, the wide angle X-ray scattering pattern exhibits intense reflections due to the crystalline parts and an amorphous halo. Usually, more than one crystalline phase can be identified as most of the semi-crystalline polymers are polymorph. WAXS experiments were implemented on the reactive blends to identify the crystalline phases α and γ that may possibly be present in the materials. Both crystalline phases are monoclinic (although the γ -phase is sometimes considered as pseudo-hexagonal). The resulting patterns were superimposed in Figure 17. The thermodynamically more stable α -

phase was identified at approximately $q = 1.45$ and 1.65 \AA^{-1} for the peaks α_1 and α_2 . The γ -phase seemed to be perceptible with the peak γ_1 at $q = 1.57 \text{ \AA}^{-1}$ between α_1 and α_2 . Moreover, a very small shoulder (noted γ_3) around 1.2 \AA^{-1} proved the presence of this negligible amount of γ -phase. The peak α_1 is attributed to the reflection of the (200) plane and corresponds to the distance between hydrogen-bonded chains in a sheet and α_2 is due to the reflections (002) and (202) planes and corresponds to the distance between two hydrogen-bonded sheets [48-50].

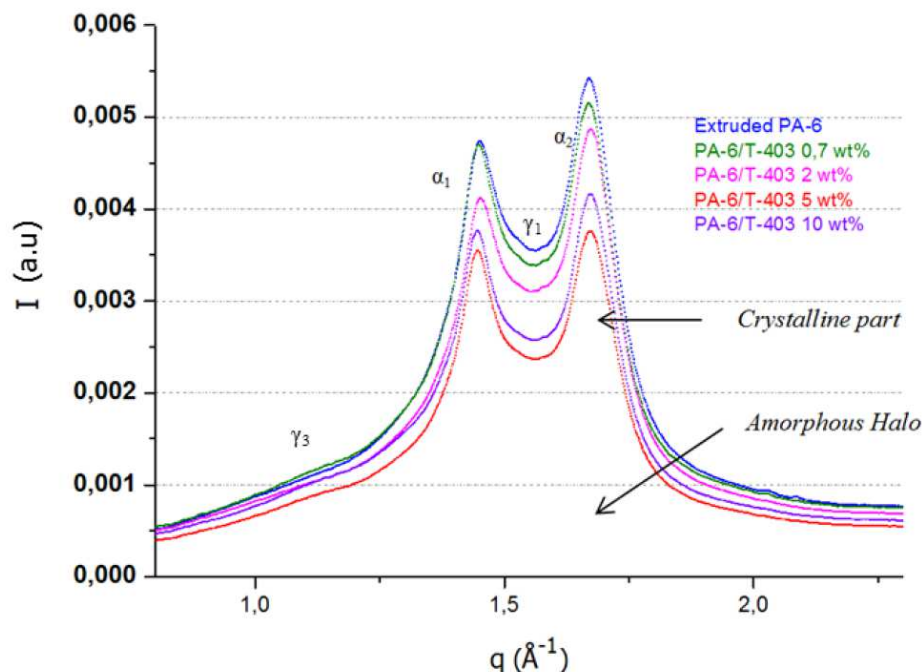


Figure 17: WAXS patterns of the formulations containing various amount of reagent T-403 (“keep colors”) (single fitting image)

As expected, the α -phase was predominant in all the formulations. Regarding the crystalline phase nature, no noticeable difference was observable between the formulations.

SAXS characterizations were implemented for a direct access to the small-scale (1 to 100 nm) morphology of the materials, that is to say, the amorphous and crystalline lamellar thicknesses (l_a and l_c respectively). In a good approximation and as detailed in the bibliographic review, a semi-crystalline polymer is made of alternating layers of crystalline and amorphous regions. This particular two-phase structure gives rise to a peak on the scattering pattern and at a define magnitude of the scattering vector (q). The peak intensity can give information on the lamellar structure regularity. Indeed, Risch et al. [51] attributed the intensity decrease of the diffraction peak to more irregularities induced by star-branching structures. The position of the diffraction peak allows for quantitative determination of the lamellae thicknesses inside the material. The peaks of diffraction obtained for each reactive blend were plotted with the Kratky representation $I(q).q^2$ vs q to obtain a distinct peak (Figure 18).

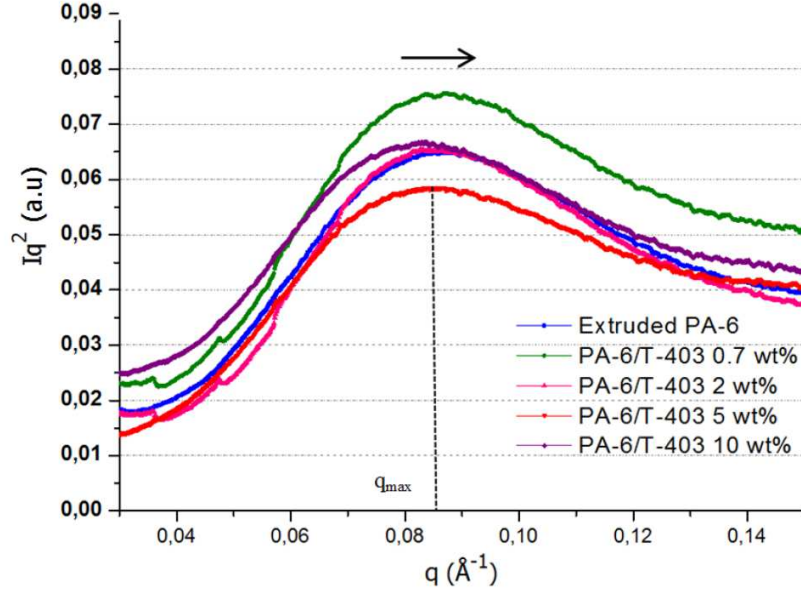


Figure 18: SAXS patterns for the reactive blends PA-6/T-403 (“keep colors”) (single fitting image)

From these patterns, it was also possible to determine the long period (L_p) from the Bragg equation (3) with the maximum peak abscissa (q_{\max}) of the curve.

$$L_p = \frac{2\pi}{q_{\max}} \quad (3)$$

The crystalline and amorphous lamellae thicknesses values could be calculated using the ideal lamellar two-phase structure [45] and knowing the degree of crystallinity (χ_c) with the simplified equations (4) and (5):

$$l_c = L_p \chi_c \quad (4)$$

$$l_a = L_p (1 - \chi_c) \quad (5)$$

χ_c was obtained by DSC and L_p , l_a and l_c were calculated and listed in the Table 8. Error on the measurement of l_c and l_a was estimated at $\pm 1-1.5$ Å. This one-dimensional layer stack model made three assumptions:

- The sample completely consists of a stack structure with crystalline and amorphous lamellae. The amorphous phase is only intraspherulitic.
- The extent of a layer is much larger than its thickness.
- Each lamella is homogeneous.

Thus, choosing a simple two-phase model for the lamellar morphology results in an overestimation of the lamellar thicknesses but can be used to compare the samples.

To have information on the respective phase composition, it is possible to consider the polymer microstructure as a three-phase model consisting of a crystalline phase, a mobile amorphous phase, and a rigid amorphous phase. With the modulated DSC results, it was possible to estimate the mobile amorphous fraction (MAF) using the equation (6) [30]:

$$\text{MAF} = \left(\frac{\Delta C_{p/\text{exp}}}{\Delta C_{p/\text{theo}}} \right) \times 100 \quad (6)$$

with, $\Delta C_{p/\text{exp}}$, the measured variation of heat capacity at the glass transition (distance between tangents at T_g) and $\Delta C_{p/\text{theo}}$, the heat capacity step for a completely amorphous polymer [$\Delta C_{p/\text{theo}}(\text{PA-6}) = 0.475 \text{ J.}(g.K)^{-1}$] [49]. The rigid amorphous fraction content can be deduced from the previous value with the following equation (7):

$$\text{RAF} = 100 - \chi_c - \text{MAF} \quad (7)$$

The MAF and RAF percentages could not be calculated for the reactive blends PA-6/T-403 containing more than 2 wt% of T-403 as the ΔC_p step was too smooth to be measured accurately. Then, the RAF thickness (l_{RAF}) could be deduced using the equation (8):

$$l_{\text{RAF}} = \frac{\text{RAF} \cdot l_c}{2 \cdot \chi_c} \quad (8)$$

with, χ_c , the crystallinity measured by DSC and l_c , the crystalline lamellae thickness obtained by SAXS [30].

Table 8: Values of the L_p , l_c and l_a measured by SAXS; χ_c , T_g and MAF/RAF obtained by classical and modulated DSC for the pure extruded PA-6 and for the PA-6/T-403 reactive blends (single fitting image)

Formulations	χ_c (%)	T_g (°C)	L_p (Å)	l_c (Å)	l_a (Å)	MAF (%)	RAF (%)	l_{RAF} (Å)	l_{MAF} (Å)
Extruded PA-6	32.5	52.0 ± 0.4	100.5	32.6	67.8	49.4	18.1	9.1	49.6
PA-6/T-403 0.7 wt%	35.2	59.3 ± 0.4	102.5	<u>36.1</u>	66.4	40.6	<u>24.2</u>	12.4	41.6
PA-6/T-403 2 wt%	35.0	52.1 ± 0.5	95.9	32.7	60.9	42.7	22.3	10.4	40.1

PA-6/T-403 5 wt%	33.2	48.8 ± 0.3	104.8	34,8	70.0	/	/	/	/
PA-6/T-403 10 wt%	30.1	/	125.6	37.8	87.8	/	/	/	/

In the literature, it has been described that the evolution of the lamellar dimension (l_c and l_a) and particularly the composition of l_a (RAF and MAF contents) are susceptible to modify the amorphous chain mobility. Indeed, if the mobile amorphous fraction not constrained by the presence of crystallites is smaller, the chain mobility in the amorphous phase is restricted by the surrounding rigid crystalline structures [30]. This is particularly observed if the amorphous layers thickness decreases below the characteristic cooperatively rearranging region (CRR) size (around 1-3 nm). Similarly, larger crystalline lamellae and higher RAF content confine the MAF and stiffen the material by their rigid nature.

In comparison to the virgin polyamide-6, for 0.7 wt% of T-403 added, the crystalline lamellae were slightly thicker (increased by 3.5 Å) and the amorphous lamellae were thinner (decreased by 1.4 Å) while the crystallinity increased. However, the l_a modifications were of low magnitude (knowing the error of 1-1.5 Å on the measurement) to explain an increase of T_g by 7.3 °C. The l_c was significantly higher but the crystalline lamellae thickness influence on the amorphous mobility has been poorly reported in the literature. A more noticeable variation regarding the PA-6/T-403 0.7 wt% sample was the MAF and RAF proportions and thicknesses. Indeed, compared to the PA-6 alone, the RAF increased from 18.1 to 24.2% and the MAF decreased from 49.4 to 40.6%. As explained previously, increasing the RAF and/or decreasing the MAF restrict some polymer chain movements due to a confined effect [27, 30]. According to the literature, this evolution might explain the glass transition shift to higher temperature. The thickening of the rigid amorphous fraction was observed in a study about the nano-phase structure of branched polymers. Alamo et al. [54] synthesized ethylene-octene copolymers with 1-butene, 1-hexene, or 1-octene as comonomers and randomly branched with a wide range of branching points (from 0.4 to 7 mol% depending on the comonomer type). They demonstrated that the RAF thickness increased with the number of branching points. As an example, for a constant M_w value of 90 000 g.mol⁻¹, the l_{RAF} of an ethylene-octene branched copolymer increased from 12 to 44 Å with 0.7 and 4.5 mol% branching points, respectively. Logically, the same observation was made regarding the RAF content. The higher l_{RAF} induced by the formation of branching points was explained by the exclusion of these branches from the crystalline lamellae. As a result, branches are accumulated at the crystalline surface (Figure 19).

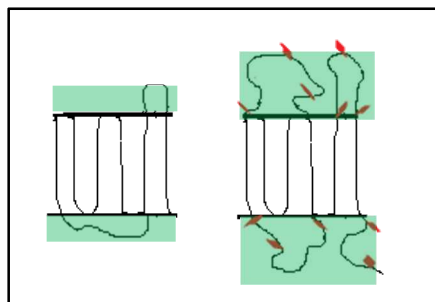


Figure 19: Schematic representation of the RAF for a linear polymer (left) and with branching points (right) (single fitting image)

In addition, as chemical modifications take place with the reagent T-403, the mobility inside the mobile and rigid phase could be changed by the new structures created. For example, the lower chain mobility in the amorphous phase might be due to the apparition of several “branching points” spaced by short segments as the glass transition corresponds to cooperative movements of short chains of 25 to 50 atoms, this is in agreement with the structures evidenced before and represented in Figure 13.

For 2 %wt of T-403, only l_a decreased significantly compared to the value obtained for polyamide-6 alone. As described in the bibliographic compilation, such a variation should induce an increase of T_g . In addition, we can see in Table 8 that this thickness decrease is mainly due to thinner l_{MAF} (l_{RAF} increases slightly). According to our reasoning, the glass transition of the formulation PA-6/T-403 2 wt% was expected to be between the one of polyamide-6 and the blend with 0.7 wt% of T-403. However, with 2 wt% of T-403, the unreacted molecules are suspected to plasticize (lower T_g) the polymer; we previously proved that only part of the T-403 reacts. To confirm this point, traction dumbbell specimens were washed in water for one week at 80 °C, so that the excess of T-403 is removed.

The washed samples were dried under vacuum at 80 °C. The T_g value was measured again and found to be at 58 °C (against 52.1 °C before this washing treatment) while the crystallinity was unchanged. Once again, this experiment demonstrated that the T_g increase can be attributed to crystalline phase composition (RAF/MAF ratio). At 2 wt%, the structural agent T-403 was already in excess to polyamide-6. The observation of the microtomed surface of this sample with an optical microscope consolidates this assumption as exudation zones of T-403 were identified (Figure 20) in the solid state.

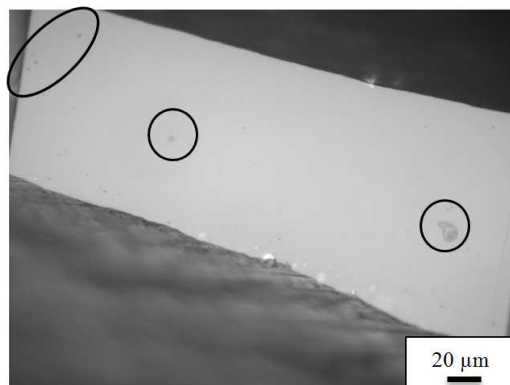


Figure 20: Optical microscope image of the microtomed surface of the blend PA-6/T-403 2 wt% (single fitting image)

Over 2 wt% of T-403, the large number of unreacted molecules promoted chain movements, plasticizing the amorphous phase. The WAXS results for 5 and 10 wt% of T-403 added were not to be considered because the interpretation might be tricky given the phase separation observed in the optical microscope images (Supplementary file 6).

Finally, the relationship described above (between the lamellae thickness/composition and the amorphous phase mobility) is plausible only if the chain orientation induced by sample injection does not affect the observed macroscopic properties. To check this parameter, samples made by melt compression (without any orientation) were analysed by SAXS and DSC. The values calculated are listed Table 9.

Table 9: Crystallinity, l_c and l_a measured by DSC and SAXS respectively for the extruded polyamide and the blend PA-6/T-403 0.7 wt% - Samples obtained by compression at 260 °C - (single fitting image)

Samples	χ_c (%)	l_c (Å)	l_a (Å)
Extruded PA-6	29.7	32.5	77.0
PA-6/T-403 0.7 wt%	32.1	35.5	75.0

If we compare these values with those obtained on injected dumbbell specimens (oriented crystallinity, given in Table 8) we can notice that χ_c , l_c , and l_a followed the same trends. Indeed, χ_c and l_c increased while the l_a decreased slightly when 0.7 wt% of T-403 was added. The degree of crystallinity for melt compressed samples was lower than that for injected samples. Similarly, DMA measurements were implemented on melt compressed samples while the modulated DSC was realized on injected specimens. Despite this difference of sample preparation, both experimental methods gave the same tendency regarding T_g . All of these observations demonstrated that the chain orientation is not responsible for the particular characteristics (T_g and χ_c) of the samples containing small concentrations of T403.

II.5. Conclusions

Two main mechanisms occur during the reactive extrusion between polyamide-6 and the triamine T-403 and they were studied in detail using model molecules and Soxhlet extracted fractions from the PA-6 based medium. On one hand, chain extension by reaction of the amino group of the T-403 on the carboxylic acid group of polyamide-6 was proved by MALDI-ToF MS and 1D/2D liquid NMR. Similarly, chain scission by transamidification was demonstrated by reaction of the reagent T-403 on the synthesized HMDA. Because of the random nature of the modified polyamide-6 with the T-403, it was difficult to further detail the molecular structure of the chains with any experimental technique (rheology model, SEC-MALLS) or models. The final material is a mixture of linear and randomly branched chains.

Both reactions induced a noticeable decrease of the amorphous phase mobility at a very low reagent concentration. This trend was confirmed by correlation of DMA and modulated DSC. The DMA showed a shift of the α - and β -relaxation towards higher temperatures while the modulated DSC demonstrated an increase of T_g .

The lower mobility of the amorphous phase, observed after the chemical reaction, was linked to the structure organization at a small scale (1 Å). The spherulites diameter was found to be around 2-3 μm and did not change with the introduction of T-403. With the addition of 0.7 wt% of triamine, the amorphous and crystalline lamellae kept their dimensions. However, considering a three-phase model, the RAF and MAF proportions were found to be modified. The higher amount of RAF (decrease of MAF respectively) hinders some polymer chain movements due to a confinement effect, and therefore increases T_g . This thicker rigid amorphous phase might be explained by accumulation of branching points at the surface of the crystal. In addition, new structures created could be a second explanation for this evolution of amorphous phase rigidity, but it was not possible to probe it experimentally. For 2 wt% of T-403 and higher concentrations, the reagent is in excess and this results in a decrease in the T_g that is caused by plasticization.

ACKNOWLEDGEMENTS

The authors thank Adrien Tauleigne for his help during the extrusion process, Fernande Da Cruz Boisson for her involvement in the interpretation of the NMR spectra, Fulchiron and Guillaume Sudre for their advices about the interpretation of the SAXS and WAXS experiments, Pierre Alcouffe for his precious formation regarding AFM measuments and Catherine Ladavière for her help regarding the MALDI-ToF mass spectrometry. The authors are grateful to the laboratory IMP/HUTCHINSON for the financial support.

FUNDING SOURCES

This work was supported by Hutchinson Company and the IMP UMR 5223 laboratory.

REFERENCES

- [1] M.N. Bureau, J. Denault, K.C. Cole, G.D. Enright, The Role of Crystallinity and Reinforcement in the Mechanical Behavior of Polyamide-6/Clay Nanocomposites, *Polym. Eng. Sci.* 42 (2002) 1897–1906. doi:10.1002/pen.11082
- [2] H. Unal, A. Mimaroglu, M. Alkan, Mechanical properties and morphology of nylon-6 hybrid composites, *Polym. Int.* 60 (2004) 56–60. doi:10.1002/pi.1246.
- [3] K. Soo, R. Nirmala, R. Navamathavan, H. Yong, Mechanical behavior of electrospun Nylon66 fibers reinforced with pristine and treated multi-walled carbon nanotube fillers, *Ceram. Int.* 39 (2013) 8199–8206. doi:10.1016/j.ceramint.2013.04.003.
- [4] L. Minkova, H. Yordanov, S. Filippi, Characterization of blends of LDPE and PA6 with functionalized polyethylenes, *Polymer.* 43 (2002) 6195–6204. doi:10.1016/S0032-3861(02)00532-3.
- [5] A. Winardi, M. Yuan, S. Gong, L.S. Turng, Core-shell rubber modified microcellular polyamide-6 composite, *J. Cell. Plast.* 40 (2004) 383–395. doi:10.1177/0021955X04047167.
- [6] G. Qiu, G. Liu, W. Qiu, S. Liu, Phase Morphology and Mechanical Properties of Polyamide-6 / Polyolefin Elastomer-g-Maleic Anhydride Blends, *J. Macromol. Sci. Part B.* 53 (2014) 615–624. doi:10.1080/00222348.2013.857536.
- [7] S. Asiaban, S. Moradian, Dyes and Pigments Investigation of tensile properties and dyeing behavior of various polypropylene / polyamide 6 blends using a mixture experimental design, *Dye. Pigment.* 92 (2011) 642–653. doi:10.1016/j.dyepig.2011.05.019.
- [8] Y. Ding, G. Chen, J. Song, Y. Gou, J. Shi, R. Jin, Q. Li, Properties and Morphology of Supertoughened Polyamide 6 Hybrid Composites, *J. Appl. Polym. Sci.* 126 (2012) 194–204. doi:10.1002/app.
- [9] M. Buccella, A. Dorigato, E. Pasqualini, M. Caldara, L. Fambri, Chain extension behavior and thermo-mechanical properties of polyamide-6 chemically modified with 1,10-Carbonyl-Bis-Caprolactam, *Polym. Eng. Sci.* 54 (2014) 158–164. doi:10.1002/pen.
- [10] M. Buccella, A. Dorigato, M. Caldara, E. Pasqualini, L. Fambri, Thermo-mechanical behaviour of polyamide 6 chain extended with 1,1'-carbonyl-bis-caprolactam and 1,3-phenylene-bis-2-oxazoline, *J. Polym. Res.* 20 (2013) 1–9. doi:10.1007/s10965-013-0225-2.
- [11] X. Chengxiang Lu, R. Ye, Y. Yang, Chemical modification of polyamide 6 by chain extension with terephthaloyl-biscaprolactam, *J. Macromol. Sci. Part C Polym. Rev.* 50 (2010) 350–362. doi:10.1080/00222341003772225.
- [12] M.T. Loontjens, K. Pauwels, F. Derks, The action of chain extenders in Nylon-6, PET, and model Compounds, *J. Appl. Polym. Sci.* 65 (1997) 1813–1819. doi:10.1002/(SICI)1097-4628(19970829)65:9.
- [13] T. Huber, P. Po, G. Pompe, R. Ha, B. Voit, S. Grutke, F. Gruber, Blends of hyperbranched poly(ether amide)s and, *Macromol. Mater. Eng.* 280 (2000) 33–40. doi:10.1002/1439-2054(20000801)280:1<33::AID-MAME33>3.0.CO;2-P.

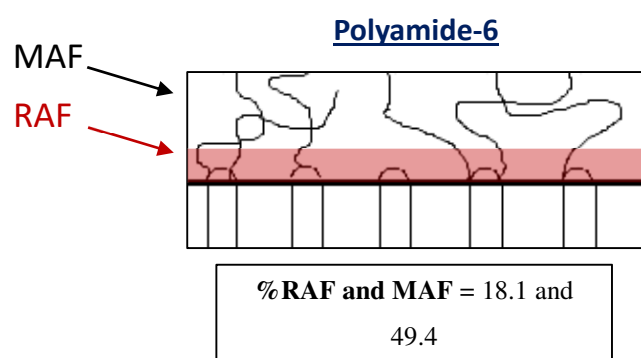
- [14] H.W. Starkweather, G.E. Moore, J.E. Hansen, T.M. Roder, R.E. Brooks, Effect of crystallinity on the properties of nylons, *J. Polym. Sci.* **21** (1956) 189–204. doi:10.1002/pol.1956.120219803.
- [15] D.C. Bassett, A. Flores, F.J. Balta, Microhardness Studies of Chain-Extended PE : I. Correlations to Microstructure, *J. Polym. Sci. Part B Polym. Phys.* **37** (1999) 3151–3158. doi:10.1002/(SICI)1099-0488(19991101)37:21<3151::AID-POLB24>3.0.CO;2-E.
- [16] S. Griessbach, R. Lach, W. Grellmann, Structure-property correlations of laser sintered nylon 12 for dynamic dye testing of plastic parts, *Polym. Test.* **29** (2010) 1026–1030. doi:10.1016/j.polymertesting.2010.09.010.
- [17] R. Simoes, J.C. Viana, G.R. Dias, A.M. Cunha, Mechanical behavior of the lamellar structure in semi-crystalline polymers, *Adv. Mater. Forum.* **732** (2013) 1006–1011. doi:10.4028/www.scientific.net/MSF.730-732.1006.
- [18] A. Menyhárd, P. Suba, Z. László, H.M. Fekete, O. Mester, Z. Horváth, G. Vörös, J. Varga, J. Móczó, Direct correlation between modulus and the crystalline structure in isotactic polypropylene, *Express Polym. Lett.* **9** (2015) 308–320. doi:10.3144/expresspolymlett.2015.28.
- [19] B. Crist, C.J. Fisher, P.R. Howard, Mechanical properties of model polyethylenes: tensile elastic modulus and yield stress, *Macromolecules.* **22** (1989) 1709–1718. doi:10.1021/ma00194a035.
- [20] Q. Huan, S. Zhu, Y. Ma, J. Zhang, S. Zhang, X. Feng, K. Han, M. Yu, Markedly improving mechanical properties for isotactic polypropylene with large-size spherulites by pressure-induced flow processing, *Polymer.* **54** (2013) 1177–1183. doi:10.1016/j.polymer.2012.12.055.
- [21] J. Huang, W. Ulrich, S. Schmauder, S. Geier, Micro-mechanical modelling of Young's modulus of semi-crystalline polyamide 6 (PA-6) and elastomer particle-modified-PA 6, *Comput. Mater. Sci.* **50** (2011) 1315–1319. doi:10.1016/j.commatsci.2010.03.012.
- [22] M.J. Doyle, On the Effect of Crystallinity on the Elastic Properties of Semicrystalline Polyethylene, *Engineering.* **4** (2000) 0–5. doi:10.1002/pen.11166.
- [23] S. Fatahi, A. Ajji, P.G. Lafleur, Correlation between different microstructural parameters and tensile modulus of various polyethylene blown films, *Polym. Eng. Sci.* **47** (2007) 1430–1440. doi:10.1002/pen.
- [24] C. Stern, A. Frick, Relationship between the structure and mechanical properties of polypropylene : Effects of the molecular weight and shear-induced structure, *J. Appl. Polym. Sci.* **103** (2007) 519–533. doi:10.1002/app.24156.
- [25] J. Dobberty, A. Hensei, C. Schick, Dielectric spectroscopy and calorimetry in the glass transition region of semi-crystalline poly(ethylene terephthalate), *J. Therm.* **47** (1996) 1027–1040. doi:10.1007/BF01979446.
- [26] R. Picciocchi, Y. Wang, N.M. Alves, J.F. Mano, Glass transition of semi-crystalline PLLA with different morphologies as studied by dynamic mechanical analysis, (2007) 575–580. doi:10.1007/s00396-006-1590-8.

- [27] P. Hong, W. Chuang, W. Yeh, T. Lin, Effect of rigid amorphous phase on glass transition behavior of poly(trimethylene terephthalate), *Polymer*. 43 (2002) 6879–6886. doi:10.1016/S0032-3861(02)00617-1.
- [28] N. Delpouve, A. Saiter, J.F. Mano, E. Dargent, Cooperative rearranging region size in semi-crystalline poly(L-lactic acid), *Polymer*. 49 (2008) 3130–3135. doi:10.1016/j.polymer.2008.04.045.
- [29] S. Charlon, L. Delbreilh, E. Dargent, N. Follain, J. Soulestin, Influence of crystallinity on the dielectric relaxations of poly(butylene succinate) and poly[(butylene succinate)-co-(butylene adipate)], *Eur. Polym. J.* 84 (2016) 366–376. doi:10.1016/j.eurpolymj.2016.09.045.
- [30] E. Parodi, L.E. Govaert, G.W.M. Peters, Glass transition temperature versus structure of polyamide 6: A flash-DSC study, *Thermochim. Acta*. 657 (2017) 110–122. doi:10.1016/j.tca.2017.09.021.
- [31] E.E. Kiziltas, H.S. Yang, A. Kiziltas, S. Boran, E. Ozen, D.J. Gardner, Thermal analysis of polyamide 6 composites filled by natural fiber blend, *BioResources*. 11 (2016) 4758–4769. doi:10.15376/biores.11.2.4758-4769.
- [32] C. Wang, F. Hu, K. Yang, T. Hu, W. Wang, R. Deng, Q. Jiang, H. Zhang, Synthesis and properties of star-branched nylon 6 with hexafunctional cyclotriphosphazene core, *RSC Adv.* 5 (2015) 88382–88391. doi:10.1039/C5RA15598C.
- [33] P.W.A. Howe, Selective diffusion spectroscopy using excitation sculpting, *Magn. Reson. Chem.* 55 (2017) 433–437. doi:10.1002/mrc.4402
- [34] X. Guo, E. Laryea, M. Wilhelm, B. Luy, H. Nirschl, G. Guthausen, Diffusion in Polymer Solutions: Molecular Weight Distribution by PFG-NMR and Relation to SEC, *Macromol. Chem. Phys.* 218 (2017) 1–10. doi:10.1002/macp.201600440
- [35] M. Nydén, M. Röding, The lognormal and gamma distribution models for estimating molecular weight distributions of polymers using PGSE NMR, *J. Magn. Reson.* 267 (2016) 54–62. doi:10.1016/j.jmr.2016.04.007
- [36] A. Rios De Anda, L.A. Fillot, D.R. Long, P. Sotta, Influence of the amorphous phase molecular mobility on impact and tensile properties of polyamide 6,6, *J. Appl. Polym. Sci.* 133 (2016) 1–9. doi:10.1002/app.43457.
- [37] A. Belous, R. Tchoudakov, A. Tzur, M. Narkis, D. Alperstein, Development and characterization of plasticized polyamides by fluid and solid plasticizers, *Polym. Adv. Technol.* 23 (2012) 938–945. doi:10.1002/pat.1988.
- [38] S.M. Queiroz, J.C. Machado, A.O. Porto, G.G. Silva, Positron annihilation and differential scanning calorimetry studies of plasticized poly(ethylene oxide), *Polymer*. 42 (2001) 3095–3101. doi:10.1016/S0032-3861(00)00668-6.
- [39] S.E. Vidotti, A.C. Chinellato, G.H. Hu, L.A. Pessan, Effects of low molar mass additives on the molecular mobility and transport properties of polysulfone, *J. Appl. Polym. Sci.* 101 (2006) 825–832. doi:10.1002/app.22855.
- [40] A.I. Suvorova, E.G. Khannanova, Molecular structure of plasticizers and antiplasticization, *Macromol. Chem. Phys.* 191 (1990) 993–998. doi:10.1002/macp.1990.021910501.

- [41] N. Kinjo, T. Nakagawa, Antiplasticization in the Slightly Plasticized Poly(vinyl chloride), *Polym. J.* 4 (1973) 143–153. doi:10.1295/polymj.4.143.
- [42] X. Ning, H. Ishida, Dynamic mechanical Analysis of RIM nylon-6, *J. Polym. Sci. Part B Polym. Phys.* 29 (1991) 1479–1492. doi:10.1002/polb.1991.090291205.
- [43] T. Vilics, H.A. Schneider, A DMA study of the suppression of the β transition in slightly plasticized PVC blends, *J. Therm. Anal.* 47 (1996) 1141–1153. doi:10.1007/BF01979453.
- [44] M. Shuster, M. Narkis, A. Siegmann, Polymeric antiplasticization of polycarbonate with polycaprolactone, *Polym. Eng. Sci.* 34 (1994) 1613–1618. doi:10.1002/pen.760342106.
- [45] O. Zhang, C. Zhang, L. Wu, L. Hu, R. Hu, Antiplasticizing effect of MOCA on poly(vinyl chloride), *J. Wuhan Univ. Technol. Mater. Sci. Ed.* 26 (2011) 83–87. doi:10.1007/s11595-011-0173-9.
- [46] A. Howard, W. Starkweather, The effect of sample preparation on the mechanical properties of nylon 66, *Polym. Eng. Sci.* 43 (2003) 759–773. doi:10.1002/pen.10063.
- [47] H. Li, M.A. Huneault, Effect of nucleation and plasticization on the crystallization of poly(lactic acid), *Polymer (Guildf)*. 48 (2007) 6855–6866. doi:10.1016/j.polymer.2007.09.020.
- [48] T. Wu, C. Liao, Polymorphism in nylon 6 / clay nanocomposites, *Macromol. Chem. Phys.* 3935 (2000) 2820–2825. doi:10.1002/1521-3935(20001201)201.
- [49] Y. Huang, D.R. Paul, Effect of molecular weight and temperature on physical aging of thin glassy Poly(2,6-dimethyl-1,4-phenylene oxide) Films, *J. Polym. Sci. Part B Polym. Phys.* 45 (2007) 1390–1398. doi:10.1002/polb.
- [50] E. Parodi, G.W.M. Peters, L.E. Govaert, Prediction of plasticity-controlled failure in polyamide 6: Influence of temperature and relative humidity, *J. Appl. Polym. Sci.* 135 (2018) 5942. doi:10.1002/app.45942.
- [51] B.G. Risch, G.L. Wilkes, J.M. Warakowski, Crystallization kinetics and morphological features of star-branched nylon-6: effect of branch-point functionality, *Polymer*. 34 (1993) 2330–2343. doi:10.1016/0032-3861(93)90817-T.
- [52] F. Defoor, G. Groeninckx, H. Reynaers, Molecular, thermal, and morphological characterization of narrowly branched fractions of 1-octene linear low-density, *Polymer*. 33 (1993) 2575–2582. doi:10.1016/0032-3861(92)90376-8.
- [53] H. Chen, P. Cebe, Investigation of the rigid amorphous fraction in Nylon-6, *J. Therm. Anal. Calorim.* 89 (2007) 417–425. doi:10.1007/s10973-007-8215-4.
- [54] R.G. Alamo, B.D. Viers, L. Mandelkern, Phase structure of random ethylene copolymers: A study of counit content and molecular weight as independent variables, *Macromolecules*. 26 (1993) 5740–5747. doi:10.1021/ma00073a031.

The manuscript is completed with 6 supplementary files in pdf format.

GRAPHICAL ABSTRACT



T-403

